

Article

# Calibration of Polarization Fields and Electro-Optical Response of Group-III Nitride Based c-Plane Quantum-Well Heterostructures by Application of Electro-Modulation Techniques

Dimitra N. Papadimitriou <sup>1,2</sup>

<sup>1</sup> National Technical University of Athens, Heron Polytechniou 9, GR-15780 Athens, Greece; DNP.NTUA@gmail.com; Tel.: +30-6974149515

<sup>2</sup> Technische Universität Berlin, Institut für Festkörperphysik, Hardenbergstr. 36, DE-10623 Berlin, Germany

Received: 15 November 2019; Accepted: 20 December 2019; Published: 27 December 2019



**Abstract:** The polarization fields and electro-optical response of PIN-diodes based on nearly lattice-matched InGaN/GaN and InAlN/GaN double heterostructure quantum wells grown on (0001) sapphire substrates by metalorganic vapor phase epitaxy were experimentally quantified. Dependent on the indium content and the applied voltage, an intense near ultra-violet emission was observed from GaN (with fundamental energy gap  $E_g = 3.4$  eV) in the electroluminescence (EL) spectra of the InGaN/GaN and InAlN/GaN PIN-diodes. In addition, in the electroreflectance (ER) spectra of the GaN barrier structure of InAlN/GaN diodes, the three valence-split bands,  $\Gamma_9$ ,  $\Gamma_{7+}$ , and  $\Gamma_{7-}$ , could selectively be excited by varying the applied AC voltage, which opens new possibilities for the fine adjustment of UV emission components in deep well/shallow barrier DHS. The internal polarization field  $E_{pol} = 5.4 \pm 1.6$  MV/cm extracted from the ER spectra of the  $\text{In}_{0.21}\text{Al}_{0.79}\text{N}/\text{GaN}$  DHS is in excellent agreement with the literature value of capacitance-voltage measurements (CVM)  $E_{pol} = 5.1 \pm 0.8$  MV/cm. The strength and direction of the polarization field  $E_{pol} = -2.3 \pm 0.3$  MV/cm of the (0001)  $\text{In}_{0.055}\text{Ga}_{0.945}\text{N}/\text{GaN}$  DHS determined, under flat-barrier conditions, from the Franz-Keldysh oscillations (FKOs) of the electro-optically modulated field are also in agreement with the CVM results  $E_{pol} = -1.2 \pm 0.4$  MV/cm. The (absolute) field strength is accordingly significantly higher than the  $E_{pol}$  strength quantified in published literature by FKOs on semipolar  $(11\bar{2}2)$  oriented  $\text{In}_{0.12}\text{Ga}_{0.88}\text{N}$  quantum wells.

**Keywords:** group-III nitrides; polarization fields; PIN-Diodes; electroreflectance; electroluminescence

## 1. Introduction

Engineering of efficient light emitting diodes (LEDs) and laser diodes (LDs) in the deep ultraviolet (UVC) range (100–280 nm) is a main goal of nanooptoelectronics and photonics [1–18]. A vast variety of applications includes water purification and availability of safe drinking water, which is a vital natural resource especially in developing countries. A proven physical disinfection method in drinking water purification is the use of ultraviolet (UV) light with wavelengths of 200–300 nm to inactivate micro-organisms. Based on the ability of UV light to function as a broad-spectrum antimicrobial agent with short contact times and minimal disinfection by-product formation, it is a viable alternative to chemical disinfectants. The wavelength of the applied UV light depends on the implemented UV emitter. Conventionally, low- and medium-pressure mercury lamps are used; however, in water purification applications, particularly in discontinuously operated, decentralized, and mobile water systems, UV light emitting diodes have certain advantages compared to conventional UV emitters: they

do not contain mercury, which may contaminate the water, and need lower voltages than conventional mercury lamps, therefore offering the option to be operated with solar cells or rechargeable batteries.

Extensive research efforts are thus devoted to the quantification and possible optimization of processes in ultra-violet light emitting diodes (UV LEDs) inclusive the control of electric fields [19–31], which ultimately affect the LED properties. Except for InGaN with very high In content, the binary members of group-III nitrides, AlN and GaN, and their alloys with InN are all wide-bandgap materials and can crystallize in both wurtzite and zinc-blende polytypes. The bandgaps of the wurtzite polytypes are direct and range from  $\approx 0.7$  eV for InN to 3.4 eV for GaN and 6.1 eV for AlN. GaN alloyed with AlN and InN may span a continuous range of direct-bandgap energies throughout much of the visible and deep into the ultraviolet spectrum. The entire visible spectrum (400–700 nm) can theoretically be covered by the InAlGaN quaternary nitrides. This makes the nitride system highly attractive for optoelectronic device applications such as LEDs, LDs, and UV-detectors and sets it on focus of intensive research and development (R&D) studies. Commercialization of bright blue and green LEDs and the possibility of yellow LEDs paved the way for the development of full-color displays with compactness, long lifetime, and relatively low power consumption. Additional possible applications include the use of LEDs in agriculture as light sources for accelerated photosynthesis and in health care for diagnosis and treatment. In this context, group-III nitrides provide an incredibly expanding material source, in particular due to their impressive optical properties being much less affected by the presence of lattice defects and dislocations than arsenides and phosphides [6,7,9]. Lateral mismatched substrates may still lead to substantial densities of misfit and threading dislocations in broad-area epitaxially deposited GaN on foreign substrates in the range of  $10^9$ – $10^{10}$   $\text{cm}^{-2}$ ; InGaN, the primary material system for efficient green and blue light emitters, however, exhibits dislocation densities typically in the order of  $10^7$ – $10^9$   $\text{cm}^{-2}$ , which in fact accelerated its commercialization. Difficulties still present in the ternary InGaN growth include the degradation of the material quality of InGaN films with increasing indium content due to the re-evaporation of indium from the instantaneous grown surface.

By precise control of the relative amounts of In and Ga in indium gallium nitride (InGaN) alloy crystals, the band gap increases smoothly and continuously as the proportions shift away from In in favor of Ga until reaching the well-established value of 3.4 eV for pure GaN. This extraordinary range of band gaps in a single kind of alloy material suggests among others its use for solar cells [8]; alloys with varying proportions of In and Ga could bracket the entire solar spectrum from the near infrared to the deep ultraviolet [13]. GaN is rather difficult to grow and to dope in order to create p-type material. Indium does not mix evenly with gallium in the alloy. Instead, it agglomerates to tiny indium-rich clusters that emit light efficiently though the material is riddled with defects. Defects usually ruin the optical properties of a semiconductor by trapping charge carriers and dissipating their energy as heat. The fact that InGaN operates as an emitter suggests that its defect tolerance may be adopted and should be of great advantage in solar cells. To exploit the alloy correspondence to the sunlight spectrum requires a multi-junction cell with layers of different composition. Lattice matching in multi-junction cells is a rather difficult task. The optoelectronic properties of nitride materials, however, show insensitivity to defect dislocations generated by the lattice mismatch. InGaN can be grown on transparent substrates including sapphire ( $\text{Al}_2\text{O}_3$ ) or silicon carbide (SiC), has tremendous heat capacity, and as other group-III nitrides is extremely resistant to radiation. These properties are ideal for the solar arrays that power communications satellites and other spacecraft. Assuming that the production costs are of the same order of magnitude as for light emitters, inexpensive nitride based efficient solar cells are expected to revolutionize space and simultaneously play a key-role in the use of solar power for terrestrial applications.

The strongest feature of group-III nitride semiconductors compared to other wide-bandgap counterparts is the heterostructure technology that it can support: quantum wells, modulation-doped heterointerfaces, and heterojunctions can all be made, in this system, giving access to new spectral regions for optical devices and new operational regimes for electronic devices [18]. The growth of InGaN quantum dots (QDs) containing multilayers appears to be profitable for pursuing higher

emission rates and broader spatial and spectral resonances. High density, self-organized InGaN/GaN quantum dots grown by plasma-assisted molecular beam epitaxy exhibit strong emission ranging from 430 to 524 nm at room temperature.

Most UV-LED heterostructures are grown on (0001) oriented c-plane sapphire substrates. Owing to the large volumes of sapphire substrates that are being used for blue LED production, sapphire wafers have become very inexpensive. Most importantly, sapphire is fully transparent across the entire UVA, UVB, and UVC spectral range because of its large bandgap energy of 8.8 eV. Considering that group-III nitrides are prepared on foreign substrates, since low-cost native substrates are not yet available, precise measurements of the mechanical, thermal, electrical, and optical properties of the group members are imperative for further advances. The common epitaxial growth of III-V nitrides in the direction normal to the c-plane of the hexagonal wurtzite structure results in polarization charges present at the layer interface and thus spontaneous electric fields affecting the optical and electrical properties of nitride material based devices [3,6,7,32–34]. The strength and direction of the internal electric fields depend also on piezoelectric fields induced by the mismatch strain between the deposited film and the substrate [35–38]. One of the most demanding physical aspects of nitride emitters is the presence of large piezoelectric fields in these materials. Because of the hexagonal lattice symmetry without a center of inversion, the piezoelectric coefficients for wurtzite nitrides are non-zero. InGaN QWs are under biaxial compressive stress due to the larger lattice constant of InGaN compared to GaN. Consequently, InGaN QWs grown along the crystallographic c-axis exhibit an internal piezoelectric field in the MV/cm range [16]. Spontaneous electric and superimposed piezoelectric fields affect the material band gap ( $E_g$ ) through the quantum confined Stark effect (QCSE) [39–41] and thus the optical properties and emission efficiency of the devices [42,43]. The strong piezoelectric field causes a current-dependent red-shift in the emission and significantly contributes to the notoriously low efficiency of green InGaN LEDs. Under controllable piezoelectricity conditions, the blue-green nitride heterostructures and QWs can be grown along crystallographic directions where the piezoelectric field is small or zero. In fact, the piezoelectric field can be cancelled out for certain oblique crystal directions, as for example in case of non- and semipolar GaN crystal orientations. For GaN optoelectronics, an entirely new approach towards different rapidly expanding activities in the area of nonpolar and semipolar nitrides has latterly been initiated, with more and more groups worldwide joining this new facet of nitride semiconductor research [30].

Direct predetermination of the material band gap and the device efficiency by selecting the semiconductor or metal element fraction is not possible. Therefore, a closer look at the nature of the inherent electric fields generated by the incorporation of a controlled heterostructure inside the intrinsic region of a PIN-LED is expected to decipher the optical response and efficiency and reveal the phenomena behind them. Accordingly, in the present work, the electro-optical response of model PIN-diodes based on group-III nitride double heterostructure (DHS) quantum wells (QWs) is studied by electroreflectance (ER) and electroluminescence (EL) spectroscopy and associated, **for calibration purposes**, with the internal electric fields. In addition, the strength and orientation of fields extracted by ER and EL modulation techniques are compared to field properties determined by capacitance-voltage measurements (CVM) on the model diodes in [44–46]. The materials used are exclusively wurtzite III-nitrides: AlN, InN, GaN, and ternary combinations of the binary compounds grown in the direction of the c-plane normal. Accurate determination of emission energies and efficiencies in dependence of bias-voltage and frequency are acquired for the correct interpretation of the electro-optical device properties, which is a prerequisite for the implementation of III nitride materials based devices with favorable design parameters and sufficient output.

## 2. Materials and Methods

InGaN/GaN and InAlN/GaN PIN-diodes with  $\text{In}_{0.055}\text{Ga}_{0.945}\text{N}$  and three different  $\text{In}_x\text{Al}_{1-x}\text{N}$  compositions ( $\text{In}_{0.15}\text{Al}_{0.85}\text{N}$ ,  $\text{In}_{0.18}\text{Al}_{0.82}\text{N}$ , and  $\text{In}_{0.21}\text{Al}_{0.79}\text{N}$ ), in a double heterostructure (DHS) grown on (0001) sapphire substrate by metalorganic vapor-phase epitaxy (MOVPE), were fabricated and

structurally characterized as described elsewhere [44–46]; the thickness of the central ternary nitride layer was determined there by high-resolution transmission electron microscopy (HRTEM). A PIN-diode with a GaN layer instead of InGaN or InAlN served as a reference sample. Schematic side-view representations of the reference and the DHS samples are illustrated in Figure 1a,b, respectively. In addition, distant and close top-view photos of the PIN-diodes are shown in Figure 1c,d, respectively. A brief description of the DHS samples is given in the following:

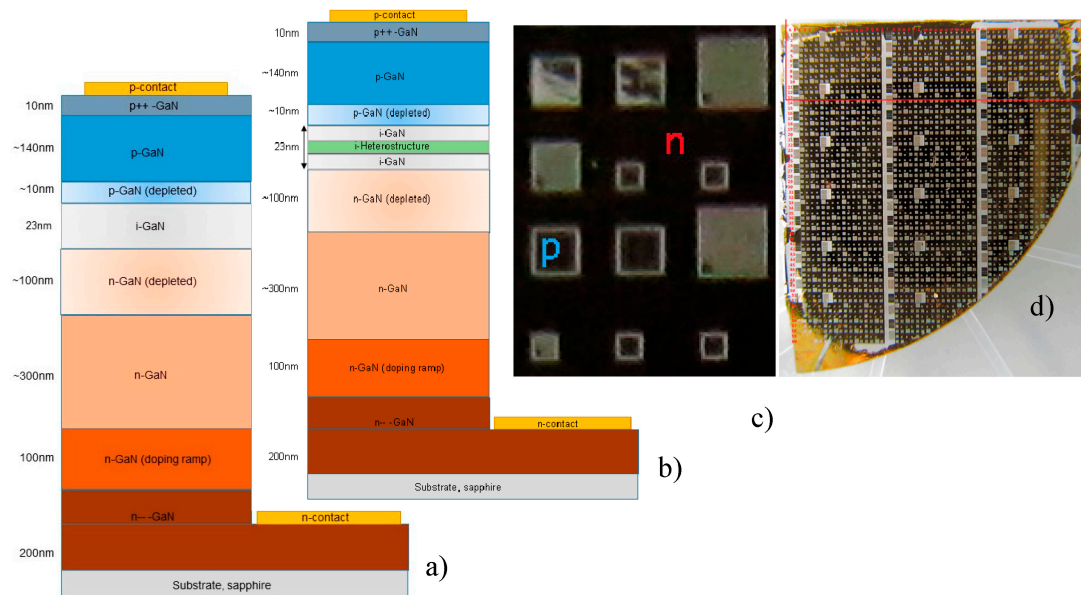


**Figure 1.** Schematic side-view representation of PIN-diodes based on (a) the GaN reference and (b) the InGaN/GaN and InAlN/GaN DHS; (c) distant and (d) close top-view photo of the PIN-diodes.

The quantum well layer of nominal thickness 9.5 nm InGaN in InGaN/GaN and 4 nm InAlN in InAlN/GaN is sandwiched between two intrinsic GaN layers (i-GaN); the total thickness of the intrinsic (unintentionally doped) region is 23 nm in both the DHS and the GaN reference. The composition of the InGaN and InAlN layers was obtained from high-resolution x-ray diffraction scans (HRXRD) of the (0002) reflection [44–46]. The adjacent n- and p-GaN layer sequences contain, at the n-side, on top of the (0001) sapphire substrate: n-doped GaN:Si layer (200 nm,  $3 \times 10^{18} \text{ cm}^{-3}$ ), graded n-doped GaN:Si layer (100 nm,  $10^{18}$ – $10^{17} \text{ cm}^{-3}$ ), low n-doped GaN:Si layer (400 nm,  $1 \times 10^{17} \text{ cm}^{-3}$ ); at the p-side: p-doped GaN:Mg (150 nm,  $3 \times 10^{18} \text{ cm}^{-3}$ ) capped with highly p-doped GaN:Mg contact layer (10 nm,  $1 \times 10^{20} \text{ cm}^{-3}$ ). Following the epitaxial heterostructure growth, PIN-diodes were fabricated by standard lithography and metallization techniques using Ni/Au as p-contact and Ti/Al/Ti/Au as n-contact [47].

The ER and EL measurements were performed using a self-developed modulation spectrometer equipped with a Xe arc spectral lamp (Oriel 75 W), two single diffraction grating monochromators, installed the first one (CVI DK240 1/4 m) in the path of the incident and the second one (SPEX 1704 1 m) in the path of the detected light beam, and a Si-diode detector. In the ER experiments, a function generator (Thurlby-Thander TG215 2 MHz) was used to modulate the InGaN/GaN and InAlN/GaN reflectance at AC voltages of 2, 4, and 6 V<sub>p-p</sub> and frequencies of 10, 30, and 60 Hz. In the EL experiments, the function generator supplied the DC voltage of the PIN-diodes ranging from the diode threshold-voltage 1.6–2.5 V up to 4 V. The PIN-diodes were contacted on a large planar n-contact and  $200 \times 200 \mu\text{m}^2$  semi-transparent p-contacts. The detected reflectance changes ( $\Delta R$ ), in the ER experiments, and the electroluminescence emission, in the EL experiments, were amplified by lock-in amplifier (Stanford Research Systems SR530) techniques.

### 3. Results and Discussion

#### 3.1. PIN-Diodes Based on InGaN/GaN DHS with 5.5% In

The electric performance of the group-III nitride semiconductor PIN-diodes analyzed in the present work by electroreflectance (ER) and electroluminescence (EL) spectroscopy in view of performance relevant electro-optical field effects was initially approached by capacitance-voltage measurements (CVM) in [44]. A brief review of the CVM measurement principles applied in [44–46] on the PIN-diodes studied by ER and EL is given in the following, since it has delivered the built-in potential  $V_{bi}$  used to evaluate the polarization fields by ER.

The capacitance  $C$  of a PIN-diode is directly related to the area and interspace of the equivalent capacitor (Equation (1)), in this case the (intrinsic) unintentionally doped ( $d_u$ ) inclusive the depletion ( $d_d$ ) region width  $d (=d_u + d_d)$  and the area  $A$  of the diode defined by the p-contact and the mesa area:

$$C = \frac{\varepsilon_0 \varepsilon_r A}{d} \quad (1)$$

Various methods utilizing the equivalent circuit characteristics can be addressed for accurate determination of the capacitance and the herewith related material and device properties, as reported in previous and recent publications [44–60]. By application of CVM techniques, the capacitance  $C$  can be determined from the current in dependence of voltage  $I(V)$  characteristics using an equivalent circuit model to evaluate the resistances [46] or alternately fitted to the impedance complex function of a PIN-diode equivalent circuit [44]:

$$Z(\omega) = R_S + \frac{1/R_P - i\omega C}{1/R_P^2 + \omega^2 C^2} \quad (2)$$

where  $C$  is the measured capacitance,  $R_S$ ,  $R_P$  are the series and parallel resistance of the equivalent circuit, respectively,  $Z(\omega)$  is given by  $Im(Z(\omega)) = |Z(\omega)|\sin\theta$  and  $|Z(\omega)| = V_{AC}/I_{AC}$  with  $V_{AC}$ ,  $I_{AC}$  the rms-values of current and voltage, respectively,  $\theta$  is the phase-shift of current with respect to voltage, and  $\omega$  is the frequency.

The main observable in CVM is the inverse of the capacitance square ( $1/C^2$ ), which depends linearly on the applied voltage [44–46]. The  $1/C^2$  dependence of the GaN reference on the applied bias-voltage is depicted in Figure 2. The slope of the  $1/C^2(V)$  curve is inversely proportional to the effective dopant concentration  $1/N_A + 1/N_D$  of the PIN-diode, which in principle defines the width  $d$  of the unintentionally doped and the depletion region ( $d = d_u + d_d$ ) [45]:

$$d = \sqrt{d_u^2 \frac{(N_D - N_i)(N_A + N_i)}{N_D N_A} + \frac{2\varepsilon_0 \varepsilon_r}{q} \left( \frac{N_D + N_A}{N_D N_A} \right) \left( V_{bi} - V - \frac{2kT}{q} - E_{pol} d_{QW} \right)} \quad (3)$$

Inserting Equation (3) in Equation (1) results in an explicit relationship of the squared inverse capacitance dependence on voltage  $1/C^2(V)$  described by Equation (4):

$$\frac{1}{C^2} = \frac{d_u^2}{\varepsilon_0^2 \varepsilon_r^2 A^2} \left( \frac{(N_D - N_i)(N_A + N_i)}{N_D N_A} \right) + \frac{2}{\varepsilon_0 \varepsilon_r q A^2} \left( \frac{N_D + N_A}{N_D N_A} \right) \left( V_{bi} - V - \frac{2kT}{q} - E_{pol} d_{QW} \right) \quad (4)$$

where  $C$  is the capacitance,  $V$  is an externally applied bias voltage,  $V_{bi}$  is the built-in potential, and  $E_{pol}$  is the polarization field of group-III nitrides.  $N_i$ ,  $N_A$ , and  $N_D$  are the intrinsic, the donor, and the acceptor dopant concentrations, respectively,  $d_{QW}$  is the thickness of the central ternary nitride (InGaN or InAlN) layer of the DHS, and  $d_u$  is the thickness of the unintentionally doped binary nitride (GaN) in the reference and ternary nitride (InGaN or InAlN) DHS based PIN-diodes.  $A$  is the p-contact area that equals the diode surface area,  $q$  is the elementary charge,  $T$  is the temperature in Kelvin, and  $k$  is the Boltzmann constant;  $\varepsilon_0$ ,  $\varepsilon_r$  are the vacuum and relative permittivity, respectively.

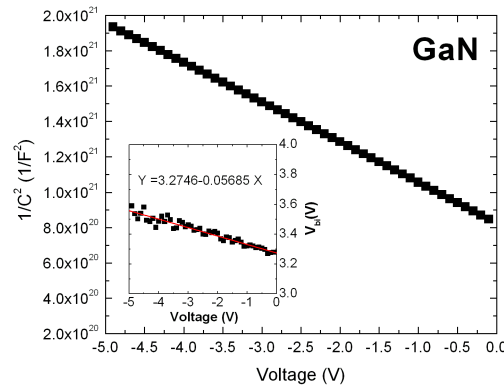


**Figure 2.** Plot of  $1/C^2(V)$  dependence of the PIN-diode based on the GaN reference [44] (inset:  $V_{bi}$  deduced from  $1/C^2(V)$  of GaN reference).

For a constant doping profile, the slope of  $1/C^2(V)$  is constant. The built-in potential  $V_{bi}$  and the polarization field  $E_{pol}$  of group-III nitrides can thus be accurately determined, as demonstrated in recent publications [44–46]:

$$V_{bi} = V + \frac{2kT}{q} + \left( \frac{\partial}{\partial V} \frac{1}{C_{ref}^2(V)} \right)^{-1} \left( \frac{d_{u,ref}^2}{\epsilon_0^2 \epsilon_r^2 A_{ref}^2} \frac{(N_D - N_i)(N_A + N_i)}{N_A N_D} - \frac{1}{C_{ref}^2} \right) \quad (5)$$

$$E_{pol} = \frac{1}{d_{QW}} \left[ V_{bi} - V - \frac{2kT}{q} + \left( \frac{\partial}{\partial V} \frac{1}{C^2(V)} \right)^{-1} \left( \frac{1}{C^2} - \frac{d_u^2}{\epsilon_0^2 \epsilon_r^2 A^2} \frac{(N_D - N_i)(N_A + N_i)}{N_D N_A} \right) \right] \quad (6)$$

The built-in potential  $V_{bi}$  deduced by CVM from the  $1/C^2(V)$  characteristic curve of the GaN reference sample exhibited a relatively weak dependence on applied voltage with  $V_{bi}(1/C^2(V=0)) = 3.28 \pm 0.22$  V, which is relevant for all processes close to equilibrium. This value is used in the determination of  $E_{pol}$  by CVM in [44,45] and by ER in this work.

The polarization field  $E_{pol}$ , which is a strictly decreasing function of the indium content, promotes interface charge generation and, therefore, the increase of the capacitance. Dependent on the sign and strength of the polarization fields, the  $1/C^2(V)$  characteristics of the  $In_xGa_{1-x}N/GaN$ ,  $x = 0.055$ , and  $In_xAl_{1-x}N/GaN$ ,  $x = 0.15, 0.18, 0.21$ , PIN-diodes are expected to be: the former higher and the latter lower than the  $1/C^2(V)$  of the GaN reference.

Group-III nitride semiconductors possess direct band gaps over a large energy range. It is the ability to create direct gap ternary alloys such as  $In_xGa_{1-x}N$ ,  $Al_xGa_{1-x}N$  or  $In_xAl_{1-x}N$  with energies beyond those of the constituent binary III nitrides that makes them profitable for use in optoelectronic devices. A band diagram of the wurtzite (WZ) crystal structure [33] in a simplified  $E(k)$  representation at  $k = 0$  ( $\Gamma$ -point) involves a non-degenerate conduction band (CB) and three separate valence split bands (VBs) upon degeneracy removal due to the hexagonal crystal field  $\Delta_{cr}$  and the spin-orbit interaction  $\Delta_{so}$ , as demonstrated in Figure 3 (left side). In reality, the bands extend over a larger range of momentum with non-parabolic dispersions and there may also be more than one confined states for both the CB and VBs. The top of the valence band is split into twofold- and single-degenerate states originated by the hexagonal crystal field  $\Delta_{cr}$ ; the former is labeled  $\Gamma_6$  and the latter  $\Gamma_1$  [61–63]. In case of GaN,  $\Gamma_6$  is higher than  $\Gamma_1$ , while in case of AlN, the  $\Gamma_1$  level is higher. The two-fold degenerate  $\Gamma_6$  state is split into  $\Gamma_9$  and  $\Gamma_7$  by the spin-orbit interaction  $\Delta_{so}$ ; the single degenerate state has also  $\Gamma_7$  symmetry. Hence, the two  $\Gamma_7$  states are mixed by the spin-orbit coupling. The hole masses of the three states:  $\Gamma_9$ ,  $\Gamma_{7+}$ , and  $\Gamma_{7-}$  have a large  $k$  dependence [61,62], and are labeled HH (heavy-holes), LH (light-holes), and CH (or SO) (crystal field split-off holes) [62,64], as shown in Figure 3. Near the band

edges, the  $E(k)$  relationship can be approximated by a quadratic equation, where  $m^*$  is the associated effective mass [65,66]:

$$E(k) = \frac{\hbar^2 k^2}{2m^*} \quad (7)$$

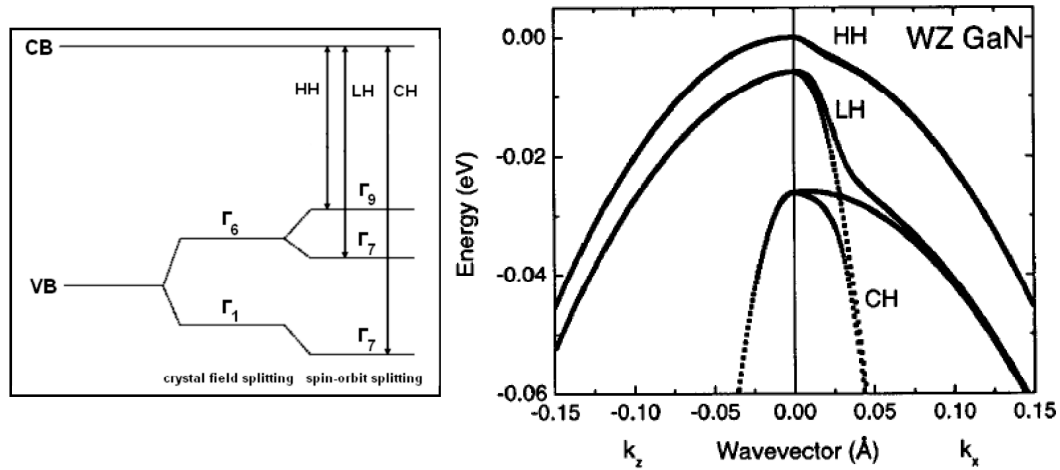


**Figure 3.** (left) Crystal field and spin–orbit interaction in wurtzite GaN [33,61–64] leading to the sub-bands of heavy (HH), light (LH), and crystal-field split-off holes (CH); (right) valence band structure of wurtzite GaN with three-split valence bands reproduced from [64] with the permission of AIP Publishing (in the wurtzite structure, crystal-field splitting appears due to the structural anisotropy parallel and normal to the c-axis).

A quantum well (QW) formed by two heterojunctions or three layers confines the free carriers in a two-dimensional (2D) system within the two well cladding barrier regions  $\Phi_b$ . The pinning of nodes at the boundaries of a well with infinite barrier height  $\Phi_b$  and width  $d_{QW}$  leads to the quantization of  $n$  sub-bands; with respect to the band edges, each sub-band has bottom energy of:

$$E_n = \frac{\hbar^2 n^2 \pi^2}{2m^* d_{QW}^2} \quad (8)$$

Carriers reside on these sub-bands instead of the band edges of the initially continuous conduction band. The effective energy gap for interband transitions inside the quantum well becomes larger than the bulk  $E_g$ .

Studies on interband excitonic transitions in wurtzite single-crystal GaN films [67], InGaN alloys [68], InGaN/GaN [69,70], and InGaAs/GaAs [71–73] single and multi-quantum well structures have already been reported, among them several using ER techniques [74–83]. However, no reports on the polarization fields of InGaN/GaN double heterostructure quantum wells determined by electro-modulation (ER) in complement with capacitance-voltage (CVM) techniques have been available up to now. The ER spectra of the PIN-diodes based on the  $\text{In}_{0.055}\text{Ga}_{0.945}\text{N}$  double quantum well and the GaN reference structure are presented in Figure 4a,b, respectively. The three-split valence bands associated with the combined effect of crystal field  $\Delta_{cr}$  and spin-orbit  $\Delta_{so}$  splitting can clearly be seen, with the respective energies,  $E_a$ ,  $E_b$ , and  $E_c$ , assigned to the sub-bands of heavy holes (HH), light holes (LH), and split-off holes (SO). The transition energies of both the binary GaN and the ternary  $\text{In}_{0.055}\text{Ga}_{0.945}\text{N}$  compounds are in the energy range expected for  $x = 0$  and  $x = 0.055$  indium content [7].

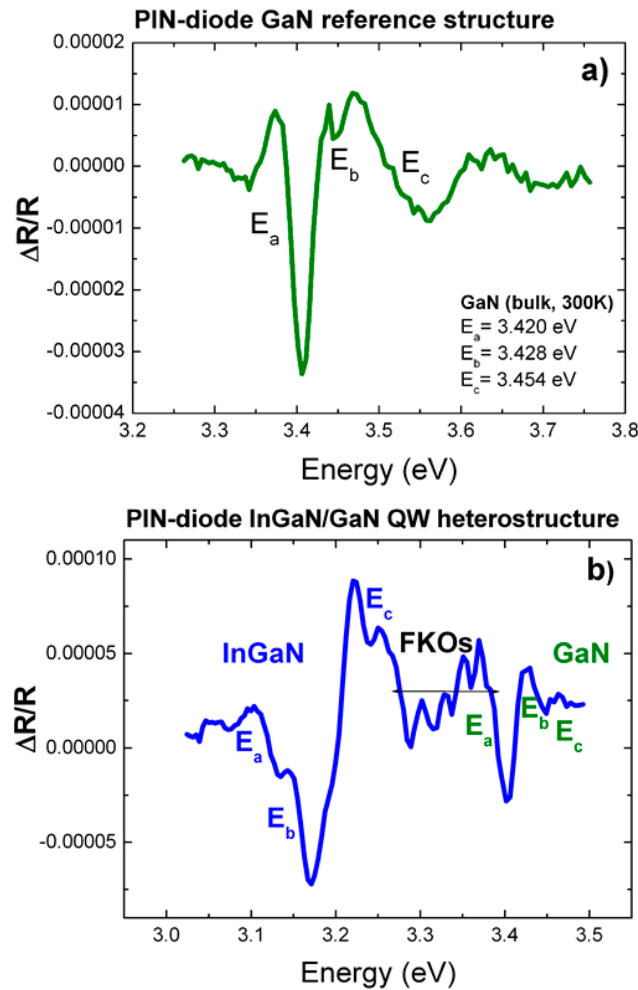


**Figure 4.** ER spectra of PIN-diodes based on (a) the GaN reference sample and (b) the  $\text{In}_{0.055}\text{Ga}_{0.945}\text{N}/\text{GaN}$  DHS with three-split valence bands  $E_a$ ,  $E_b$ , and  $E_c$  of the wurtzite crystal structure.

Extensive research studies of the optical properties of bulk semiconductors and semiconductor microstructures under the application of modulation spectroscopy, in the past, are being renewed at present [84–93]. Electromodulation is the most useful of various optical modulation methods since it yields, in general, the sharpest spectral features and is sensitive to surface (interface) electric fields. In the presence of relative stark internal fields, oscillations at energies above the band gap energy are ascribed to the Franz–Keldysh effect [94–99]. Oscillations at energies 3.29–3.37 eV, in Figure 4b, are thus Franz–Keldysh oscillations (FKOs) of barrier regions of the InGaN/GaN DHS stimulated in the intermediate field regime. The main features of these spectra are the high-electric-field induced Franz–Keldysh oscillations above the  $E_0$  transition, the broadening of the excitonic  $E_0$  transition, and the clearly observed  $E_0 + \Delta E_0$   $\text{In}_{0.055}\text{Ga}_{0.945}\text{N}$  direct transition between the spin-orbit splitted valence band and the conduction band. The extrema of FKOs are given by [90,94,95]:

$$m_{FKO}\pi = \phi + \frac{4}{3} \left( \frac{E_m - E_0}{\hbar\Theta} \right)^{\frac{3}{2}} \quad (9)$$

where  $m_{FKO}$  is the index of the  $m$ -th extremum,  $\phi$  is an arbitrary phase factor,  $E_m$  is the photon energy of the  $m$ -th oscillation,  $E_0$  is the energy gap, and  $\hbar\Theta$  is the electro-optic energy given by:

$$(\hbar\Theta)^3 = \frac{q_e^2 \hbar^2 F^2}{2\mu_{//}} \quad (10)$$



with  $q_e$  the electron elementary charge and  $\mu_{//} (= m_e^* m_{hh}^* / (m_e^* + m_{hh}^*))$  the reduced interband effective mass for the electron and heavy-hole pair in the direction of  $F$ . The electric field  $F$  can, therefore, be obtained directly from the period of the FKO, if  $\mu_{//}$  is known.

A plot of the FKO extrema  $E_m$  as a function of redefined index  $m = [(3/4)m_{FKO}\pi]^{2/3}$  (Figure 5) yields a straight line with slope  $\hbar\Theta = 0.01536$  eV and ordinate-intercept the  $E_a$  transition energy (fundamental gap energy  $E_0$ ) of the  $\text{In}_{0.055}\text{Ga}_{0.945}\text{N}/\text{GaN}$  quantum well heterostructure,  $E_0 = 3.260 \pm 0.002$  eV, averaged over several measurements,  $\langle E_0 \rangle = 3.248 \pm 0.006$  eV. The bandgap energies of III–V ternary compounds have an approximately quadratic dependence on the alloy composition  $x$ :  $E_0(\text{A}_x\text{B}_{1-x}\text{C}) = x E_0(\text{AC}) + (1 - x) E_0(\text{BC}) + p(\text{A-B}) x(1 - x)$  [7,100]. According to recently published literature on the fundamental properties of III–V ternary and quaternary alloys [100], the band-gap energies of the related III–V binaries at 300 K and the bowing parameter  $p(\text{A-B})$ , in case of  $\text{A}_x\text{B}_{1-x}\text{C} = \text{In}_x\text{Ga}_{1-x}\text{N}$ , are:  $E_0(\text{InN}) = 1.1$  eV,  $E_0(\text{GaN}) = 3.42$  eV, and  $p(\text{In-Ga}) = -1.64$ . Considering that the (fundamental) energy band gap of bulk InGaN with 5.5% In-fraction is  $E_g(\text{In}_{0.055}\text{Ga}_{0.945}\text{N}) = 3.207$  eV, the excess energy  $\Delta E = (3.248 - 3.207 \text{ eV}) = 0.041 \pm 0.006$  eV originates from the band gap broadening of the InGaN/GaN QW heterostructure as described by Equation (8). For the respective interband transition, rearrangement of the terms in Equation (8) yields the width  $L_W$  ( $n = 1$ ) of the InGaN/GaN quantum well heterostructure:

$$L_W = \frac{h}{\sqrt{8\mu_{//} \Delta E}} \tag{11}$$

where  $\Delta E = 0.041$  eV ( $1 \text{ eV} = 1.602 \times 10^{-19}$  J) is the band broadening due to quantum confinement and  $\mu_{//}$  is the reduced effective mass in  $\text{In}_{0.055}\text{Ga}_{0.945}\text{N}$  set equal to  $\mu_{//}$  in GaN.

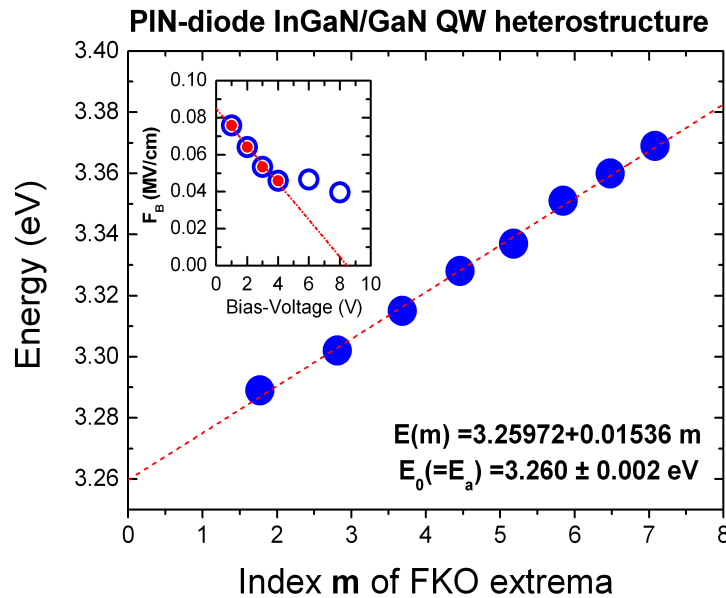


**Figure 5.** Linear fitting of the Franz–Keldysh oscillation (FKO) extrema of the ER spectrum of the  $\text{In}_{0.055}\text{Ga}_{0.945}\text{N}/\text{GaN}$  DHS of Figure 4b (inset: electric field in the barrier and depletion region interface in dependence of bias-voltage).

For the calculation of the internal electric field  $F$  with Equation (10) and the QW width  $d_{QW} (= L_W)$  with Equation (11), the effective mass of electrons and holes in  $\text{In}_{0.055}\text{Ga}_{0.945}\text{N}$  was set equal to  $m_e^* = 0.20m_0$  and  $m_{hh}^* = 2.20m_0$  in GaN [101], with the free electron rest mass  $m_0 = 9.109 \times 10^{-31}$  kg, the elementary charge  $q_e = 1.602 \times 10^{-19}$  C, and Planck’s constant  $\hbar = h/2\pi$ ,  $h = 6.626 \times 10^{-34}$  m<sup>2</sup> kg/s.

The calculated QW width  $d_{QW} = d_{\text{InGaN}} = 7.09 \pm 1.04$  nm converges to the value of nominal thickness ( $9.5 \pm 0.5$  nm) striven.

The calculated values of the  $\text{In}_{0.055}\text{Ga}_{0.945}\text{N}/\text{GaN}$  field  $F$  in the barrier interface region ( $F = F_B$ ) are plotted in the inset of Figure 5 in dependence of the modulation voltage. FKOs are usually related to surface/interfaces, thus barrier regions of heterojunctions, and, in this case, to the field  $F_B$  existing at the  $\text{InGaN}/\text{GaN}$  interface barrier, which is expected to be weaker than the (total) field  $E_{pol}$ . For a pin structure, there are three contributions to the FKOs [99]: one from the unintentionally doped QW barriers that have a uniform electric field of  $F_B$ ; the other two from the depletion regions, at the p- and n-sides, that have non-uniform electric fields with the maximum fields equal to  $F_B$ . Under small AC modulation, the period of the FKOs originating in the depletion region is determined by the maximum electric field  $F_B$  [95,99].

In general, if a quantum well (QW) structure is incorporated in the intrinsic region of a p-i-n diode, an external field can be applied, leading to an expression of the voltage drop across the DHS [72]:

$$V_{appl} + V_{bi} + E_w L_w + E_b L_b = 0 \tag{12}$$

where  $V_{appl}$  and  $V_{bi}$  are the externally applied bias and the built-in potential,  $L_w(L_b)$  and  $E_w(E_b)$  are the well (barrier) length and well (barrier) field, respectively.

The QW-structure, however, has an internal envelope electric field,  $\vec{E}_{int}$ , across the DHS that opposes the conventional built-in field [73]:

$$E_{int} = \frac{E_w L_w + E_b L_b}{L_w + L_b} \tag{13}$$

As a result, the energy minima and envelope functions of all sub-bands supported by the QW are strongly modified relative to the ideal flat-band case ( $\vec{E}_w = \vec{E}_b = 0$ ) through the quantum-confined Stark effect.

The majority of approaches to determine the internal electric field have relied upon counterbalancing the quantum-confined Stark effect with an **externally applied reverse bias**  $V_{appl}$  and measuring properties of the quantum well as a function of this applied reverse bias. At low bias, the well is skewed due to the internal field. At a critical bias, the contributions from the applied bias and the internal field are equal and opposite [28]. The total field ( $\vec{F} = \vec{E}_{total}$ ) in the DHS is approximated as follows:

$$E_{total} = E_{int} - V_{appl}/(d_u + d_d) \tag{14}$$

$$E_{int}(d_u + d_d) = V_{bi} - E_w L_w - E_b L_b \tag{15}$$

$$d_u = L_w + L_b \tag{16}$$

where  $\vec{E}_{int}$  represents the fields due to the piezoelectric effect and the spontaneous polarization in the unintentionally doped (intrinsic) and depletion regions with spatial widths  $d_u$  and  $d_d$ , respectively, and  $V_{bi}$  is the built-in voltage from the p-n junction.

Considering that on (0001) substrates the electric fields in the wells and barriers are of equal strength ( $E_w = E_b = E_{pol}$ ) [72], Equations (14)–(16) yield:

$$F = E_{total} = \frac{(V_{bi} - V_{appl} - E_{pol}d_u)}{(d_u + d_d)} \tag{17}$$

Hence, for a QW sandwiched inside a p-n junction (p-i(QW)-n), the electric field  $\vec{F}(=\vec{E}_{total})$  is related to the polarization field  $\vec{E}_{pol}$  and bias voltage  $V_{appl}$  by Equation (17). The first term of Equation (17) is the background field written as the total voltage drop divided by the distance ( $d_u + d_d$ ) over which that drop occurs. The externally applied voltage is negative for reverse bias.

At a flat-barrier (FB) condition, the electric field in the barrier-interface region ( $\vec{F} = \vec{F}_B$ ) is zero and the polarization field  $\vec{E}_{pol}$  can be determined by solving Equation (17) for  $F_B (= F) = 0$  [99]:

$$E_{pol} = \frac{V_{bi} - V_{FB}}{d_u} \tag{18}$$

where  $V_{FB}$  is the bias voltage at flat-barrier condition. In the vicinity of flat-barrier,  $F_B (= F)$  approaches a linear relation with bias voltage.

For the  $\text{In}_{0.055}\text{Ga}_{0.945}\text{N}/\text{GaN}$  field studied in this work, the flat-barrier condition is sustained for voltages below the emission threshold voltage of the respective PIN-diode of 4 V AC, as demonstrated in Figure 6. The field is maintained in the voltage-plateau 4–6 V, and is overwhelmed above 8 V, where FKOs are almost buried in the superimposed UV emission. In the inset of Figure 5, a fit of the electric field in dependence of voltage  $F_B(V)$  with a straight line up to  $F_B = 0$  intersects the  $x$ -axis at a flat-barrier voltage of  $V_{FB} = 8.47 \pm 0.58$  V. Using the built-in potential value selected at 0 V in capacitance-voltage measurements  $V_{bi} = 3.28 \pm 0.22$  V (part 3 Results and Discussion), since all equations were derived close to equilibrium [65], and  $d_u = 23.0 \pm 2.0$  nm (Figure 1b), the polarization field in the  $\text{In}_{0.055}\text{Ga}_{0.945}\text{N}/\text{GaN}$  DHS is found to be  $E_{pol} = -2.26 \pm 0.33$  MV/cm in the same direction as the built-in field.

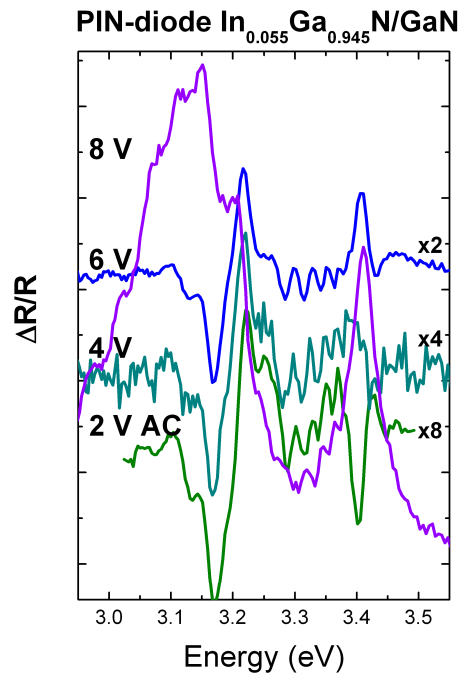


**Figure 6.** ER spectra of PIN-diodes based on  $\text{In}_{0.055}\text{Ga}_{0.945}\text{N}/\text{GaN}$  DHS in dependence of AC modulation voltage.

The field  $F$  experienced by carriers with concentration  $N_{\text{InGaN}}$  and charge  $q_e$  across the  $\text{InGaN}/\text{GaN}$  DHS under application of an external voltage  $V_{AC}$  can be approximated by [90]:

$$F = \sqrt{\left(\frac{2q_e N_{\text{InGaN}}}{\epsilon_{\text{InGaN}} \epsilon_0}\right) \left(V_{bi} - V_{AC} - \frac{kT}{q_e}\right)} \tag{19}$$

where  $\epsilon_{\text{InGaN}} = 10.518$  is the relative permittivity of the intrinsic  $\text{InGaN}$  layer [26] and  $\epsilon_0 = 8.854 \times 10^{-12}$  F/m is the vacuum permittivity. The field  $F$  modulated with  $V_{AC} = 2$  V is according to Equation (10)  $F = 4.18 \times 10^6$  V/m.

The carrier concentration determined by Equation (20) after term-reorder of Equation (19):

$$N = \frac{(\epsilon_{InGaN} \epsilon_0 F^2)}{2q_e (V_{bi} - V_{AC} - kT/q_e)} \quad (20)$$

is  $N_{InGaN} = 4.04 \times 10^{15} \text{ cm}^{-3}$ , which is a realistic value considering that the InGaN layer is unintentionally doped with dopant concentration typically in the range  $10^{15}$ – $10^{16} \text{ cm}^{-3}$ , and that FKO are generally observed in this doping range [90].

Oscillations at energies below the band gap energy, as demonstrated in Figure 7, are thickness interferences [102–105] and can be used to determine the thickness of the GaN layer, alternately, the thickness of the GaN/InGaN/GaN layer region penetrated by the incident beam:

$$t = \frac{N\lambda_1\lambda_2}{2(\lambda_1 - \lambda_2) \sqrt{n_f^2 - (\sin \theta)^2}} \quad (21)$$

where  $t$  is the thickness of the film,  $\lambda_1$  and  $\lambda_2$ ,  $\lambda_1 > \lambda_2$ , are the begin- and end-wavelength of the spectral region where the oscillations appear,  $N$  is the number of oscillations within this region,  $n_f$  is the refractive index of the film, and  $\theta$  is the angle between the incident beam and the normal to the surface [104]. For  $N = 10$  oscillations in the range 2.583–3.107 eV (400–480 nm), at angle of incidence  $\theta = 45^\circ$ , a thickness of  $t = 4.5 \text{ }\mu\text{m}$  was calculated by inserting  $n_{InGaN} \approx n_{GaN} = 2.82$  [89,106–109] in Equation (21), which accounts for both the GaN and the InGaN DHS based PIN-diode layer thickness in Figure 1a,b.

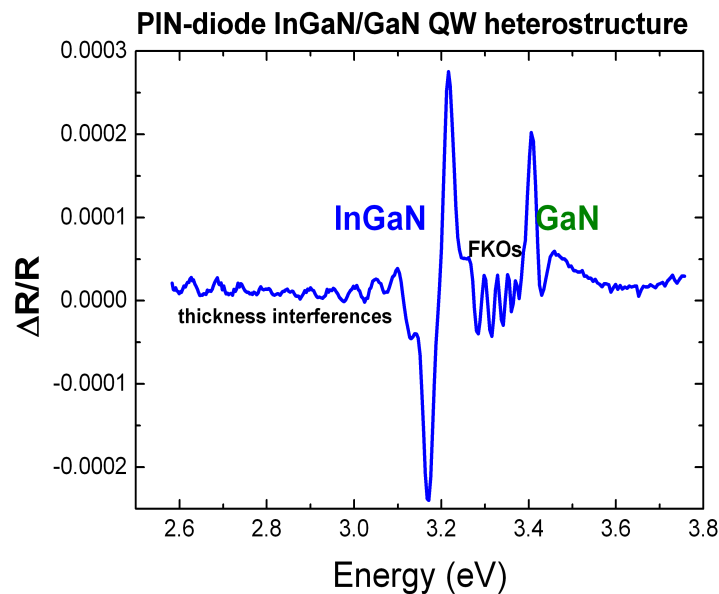


**Figure 7.** ER spectrum of PIN-diode based on  $\text{In}_{0.055}\text{Ga}_{0.945}\text{N}/\text{GaN}$  double heterostructure quantum-well with thickness interferences at energies below the band gap energy of  $\text{In}_{0.055}\text{Ga}_{0.945}\text{N}$ .

### 3.2. PIN-Diodes Based on $\text{InAlN}/\text{GaN}$ DHS with 15, 18, 21% In

Opposite to the  $\text{In}_x\text{Ga}_{1-x}\text{N}/\text{GaN}$  DHS with shallow well/high barrier, in case of the  $\text{In}_x\text{Al}_{1-x}\text{N}/\text{GaN}$  DHS with deep well/shallow barrier, no Franz–Keldysh oscillations were observed. The  $E_a$ ,  $E_b$ , and  $E_c$  transition energies of the GaN barrier showed instead a remarkable dependence on the applied modulation voltage in the range of 2–6 V AC, as depicted in Figure 8a. An ER spectrum with good resolved transitions between the three-split valence band and the conduction band of  $\text{In}_x\text{Al}_{1-x}\text{N}$  was recorded only in case of the PIN-diode based on the  $\text{In}_{0.21}\text{Al}_{0.79}\text{N}/\text{GaN}$  DHS with the maximum of the investigated indium fractions of 21% In; the respective transition energies of  $E_a = 3.695 \text{ eV}$ ,  $E_b =$

3.723 eV, and  $E_c = 3.748$  eV can be evidenced in Figure 8b. An approximated value of the polarization field in the quantum well and the barrier interface can be deduced directly from the measured  $E_a$  energy as  $E_{pol}^W = E_a/d_{QW} = 3.695 \text{ V}/4 \text{ nm} = 9.24 \text{ MV/cm}$  and  $E_{pol}^B = E_a/d_u = 3.695 \text{ V}/23 \text{ nm} = 1.61 \text{ MV/cm}$ , respectively. The mean value of  $E_{pol} = 5.42 \pm 1.63 \text{ MV/cm}$  obtained by ER is in excellent agreement with the value determined by CVM as  $E_{pol} = 5.1 \pm 0.8 \text{ MV/cm}$  [45]. Line-shape analysis of the ER spectra would exceed the objectives of the present work.

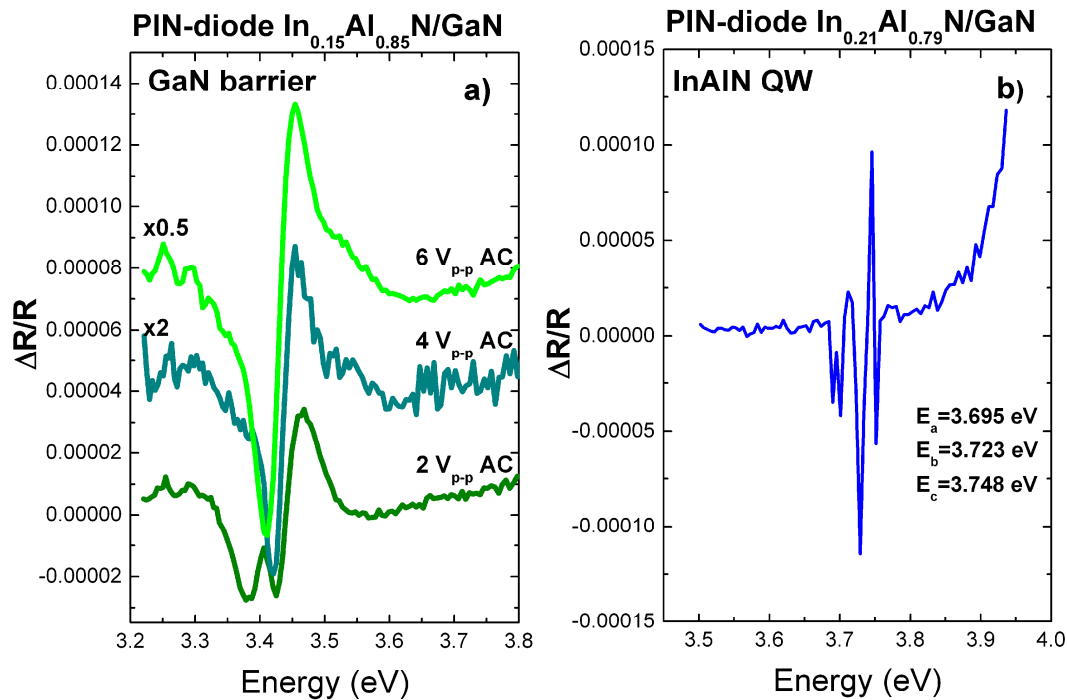


**Figure 8.** ER spectra of PIN-diodes based on  $\text{In}_x\text{Al}_{1-x}\text{N}/\text{GaN}$  DHS: (a) selection of transition energies  $E_a$ ,  $E_b$ , and  $E_c$  of the GaN barrier in  $\text{In}_{0.15}\text{Al}_{0.85}\text{N}/\text{GaN}$  DHS by variation of AC bias-voltage and (b) transition energies  $E_a$ ,  $E_b$ , and  $E_c$  of InAlN in  $\text{In}_{0.21}\text{Al}_{0.79}\text{N}/\text{GaN}$  DHS.

### 3.3. Results of Comparative Studies of Polarization Fields by Electroreflectance (ER) Spectroscopy and Capacitance-Voltage Measurements (CVM)

The values of the polarization fields  $E_{pol}$  of the  $\text{In}_{0.055}\text{Ga}_{0.945}\text{N}$  and the  $\text{In}_{0.15}\text{Al}_{0.85}\text{N}$ ,  $\text{In}_{0.18}\text{Al}_{0.82}\text{N}$ ,  $\text{In}_{0.21}\text{Al}_{0.79}\text{N}$  DHS determined by ER in this work are compared, in Figure 9, with the values determined by CVM in [44–46] and with theoretically predicted values [19,26,38]. The analytical approach indicates moderate polarization fields of  $\text{In}_{0.055}\text{Ga}_{0.945}\text{N}$  ( $-1.2 \pm 0.4 \text{ MV/cm}$ ) and high polarization fields of  $\text{In}_{0.15}\text{Al}_{0.85}\text{N}$  ( $5.9 \pm 0.8 \text{ MV/cm}$ ),  $\text{In}_{0.18}\text{Al}_{0.82}\text{N}$  ( $5.4 \pm 0.9 \text{ MV/cm}$ ), and  $\text{In}_{0.21}\text{Al}_{0.79}\text{N}$  ( $5.1 \pm 0.8 \text{ MV/cm}$ ) determined by CVM. The (total) polarization field of  $\text{In}_{0.055}\text{Ga}_{0.945}\text{N}$  ( $-2.3 \pm 0.3 \text{ MV/cm}$ ) determined by ER is in agreement, within the experimental and calculation errors, with the CVM result. The same holds for the polarization field of  $\text{In}_{0.21}\text{Al}_{0.79}\text{N}$  ( $5.4 \pm 1.6 \text{ MV/cm}$ ) extracted from the ER spectra. The field values predicted theoretically by F. Bernardini et al. [19], O. Ambacher et al. [26], and A. F. Wright [38] are of the same order of magnitude. Nevertheless, they also foresee a field decrease with the increase of the In-content higher than experimentally measured, which could be indicative of an underestimation of the piezoelectric field contribution to the total polarization field. On the other hand, the experimental error is quite large, which is partially due to the particularly small InAlN and InGaN layer thickness of 10 nm maximal.

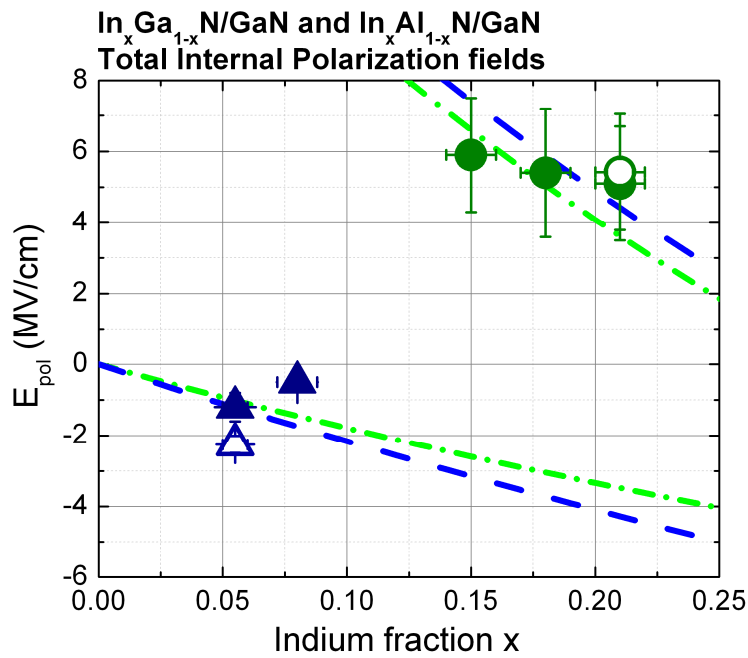


**Figure 9.** Comparison of the polarization field values  $E_{pol}$  of  $In_{0.055}Ga_{0.945}N$  DHS (open triangle) and  $In_{0.21}Al_{0.79}N$  DHS (open circle) determined by ER in this work with the field values of  $In_{0.055}Ga_{0.945}N$  [44],  $In_{0.08}Ga_{0.92}N$  DHS [46] (full triangles) and  $In_{0.15}Al_{0.85}N$ ,  $In_{0.18}Al_{0.82}N$ ,  $In_{0.21}Al_{0.79}N$  DHS [45] (full circles) determined by CVM, and with theoretically predicted values [19,38] (dashed line) and [26] (dot-dashed line).

### 3.4. Comments on Formalism of Polarization Field Determination

A basic property of nitride semiconductors, which directly affects the electronic, transport, and optical properties of heterostructures, is the presence of strong spontaneous  $P_{SP}$  and piezoelectric  $P_{PE}$  polarizations. The orientation of both  $P_{SP}$  and  $P_{PE}$  polarizations along the c-axis depends on the sequence of atomic layers in the crystal. The compositional dependence and large magnitude of  $P_{SP}$  and  $P_{PE}$  play an important role in the optoelectronic device physics of nitride semiconductors due to the associated polarization charge distributions. A surface charge distribution results in the formation of an electrostatic field perpendicular to the interface. In heterostructures, polarization charges are induced on each heterojunction and can produce large internal electric fields that strongly bend the conduction- and valence-band edges near the interface. The electric fields produced by the polarization charges in heterostructures can be evaluated using principles of electrodynamics. In case of multiple-quantum-well (MQW) structures, which are used routinely in most optoelectronic device applications, the well and barrier materials can be InGaN and GaN, AlGaN and GaN, or InAlN and GaN, as in the present case, and their properties are denoted by the subscripts w and b, respectively.

In accordance with Maxwell’s theory of the electromagnetic field, the electric displacement  $\vec{D}$  of a material of dielectric permittivity  $\epsilon$  subjected to electrical polarization  $\vec{P}$  under the influence of an (external) electric field  $\vec{E}$  is given by:

$$\vec{D} = \epsilon \vec{E} = (1 + \chi) \vec{E} = \vec{E} + \chi \vec{E} = \vec{E} + \vec{P} \tag{22}$$

Continuity of the displacement flux across each interface of a well-barrier pair requires that:

$$\vec{E}_w + \vec{P}_w = \vec{E}_b + \vec{P}_b \tag{23}$$

A simple analytical solution for the fields in well  $\vec{E}_w$  and barrier  $\vec{E}_b$  can be obtained in the limit of an infinitely periodic structure, where the intrinsic voltage drop across each well/barrier pair must be zero [110]:

$$\vec{E}_w L_w + \vec{E}_b L_b = 0 \tag{24}$$

with  $L = L_w + L_b$  being the layer thickness.

Combining Equations (23) and (24) yields the polarization-induced built-in electric field in the well layers:

$$\vec{E}_w = \frac{(\vec{P}_b - \vec{P}_w)L_b}{L_w + L_b} \tag{25}$$

Very large values of up to a few MV/cm are typically computed for these fields in c-plane nitride heterostructures. As a result, the energy minima and envelope functions of all sub-bands supported by the QWs are strongly modified relative to the ideal flat-band case ( $\vec{E}_w = \vec{E}_b = 0$ ) through the quantum-confined Stark effect. The existence of strong piezoelectric fields results thus in a red-shift of the excitonic transitions within strained QWs. Application of an external bias can modulate these fields to obtain a blue-shift of the absorption edge.

If a multiple-quantum-well (MQW) structure is incorporated in the intrinsic region of a p-i-n diode, an external field can be applied leading to the expression [72]:

$$E_w L_w + E_b L_b = -(V_{bi} + V_{appl}) \tag{26}$$

where  $V_{appl}$  and  $V_{bi}$  are the applied and built-in potentials, respectively.

Combining Equations (23) and (26) gives the polarization-induced built-in electric field in the well layers under the influence of an external field:

$$E_w L_w + E_w L_b + (P_w - P_b)L_b = -(V_{bi} + V_{appl}) \tag{27}$$

On (100) substrates, the electric fields in the wells and barriers are of equal strength, while, for structures grown on substrates other than (100), the piezoelectric field  $\vec{E}_p$  can be expressed as [72]:

$$\vec{E}_p \equiv \vec{E}_w - \vec{E}_b \tag{28}$$

Taking into consideration Equation (23), it can also be expressed as:

$$\vec{E}_p \equiv \vec{P}_b - \vec{P}_w \tag{29}$$

By substitution of Equation (29) into Equation (27), the well and barrier fields for a p-i-n structure, grown so that the p-doped layer is uppermost, are:

$$E_w = \frac{-(V_{bi} + V_{appl}) + (P_b - P_w)L_b}{L_w + L_b} = -\frac{(V_{bi} + V_{appl})}{L} + \frac{E_p L_b}{L} \tag{30}$$

$$E_b = \frac{-(V_{bi} + V_{appl}) - (P_b - P_w)L_w}{L_b + L_w} = -\frac{(V_{bi} + V_{appl})}{L} - \frac{E_p L_w}{L} \tag{31}$$

Equations (30) and (31) indicate that for a given external bias  $V_{appl}$ , the well  $\vec{E}_w$  and barrier  $\vec{E}_b$  fields are dependent on the i-region length and the lengths of the barrier and the well material, respectively. The magnitude of the overall well field is reduced as more wells are incorporated into an

i-region of a p-i(MQW)-n diode structure of a given thickness; likewise the barrier fields must increase accordingly:

$$E_w = -\frac{(V_{bi} + V_{appl})}{L} + \frac{E_p nL_b}{L} \tag{32}$$

$$E_b = -\frac{(V_{bi} + V_{appl})}{L} - \frac{E_p nL_w}{L} \tag{33}$$

and

$$L = n(L_w + L_b) \tag{34}$$

where  $L_w$  is the length of a single QW and  $n$  is the number of wells.

Using Equation (34), Equation (32) can be then rewritten as:

$$E_w = -\frac{(V_{bi} + V_{appl})}{L} + \frac{E_p (L - nL_w)}{L} = -\frac{(V_{bi} + V_{appl})}{L} - \frac{E_p nL_w}{L} + E_p \tag{35}$$

In the absence of illumination, the electric field  $\vec{E}_w$  within the wells amounts [73]:

$$E_w = -\frac{V_{bi}}{L} + \frac{E_p (L - nL_w)}{L} = -\frac{V_{bi}}{L} - \frac{E_p nL_w}{L} + E_p \tag{36}$$

The internal electric field is determined by counteracting the quantum-confined Stark effect (QCSE) with an externally applied reverse bias; the reverse bias  $V_{appl}$  acts to oppose the internal field and attenuate the induced QCSE. A decrease of the internal polarization field  $\vec{E}_p$  implies cancellation of the piezoelectric field  $\vec{E}_{piezo}$  by the reverse bias. The piezoelectric field is set, in principle, against the built-in  $V_{bi}$  and reverse bias field  $V_{appl}$ .

In [69], the total internal field ( $\vec{E}_{total}$ ) in the well layer was approximated as follows:

$$E_{total} = E_i - \frac{V_{appl}}{(d_u + d_d)} + E_{piezo} \tag{37}$$

$$V_{bi} = E_i(d_u + d_d) + E_{piezo}NL_w \tag{38}$$

where  $V_{bi}$ ,  $V_{appl}$ ,  $\vec{E}_{piezo}$ , and  $\vec{E}_i$  represent the built-in potential, the applied voltage, the piezoelectric field, and the internal field in the undoped and depletion regions, respectively. The thicknesses of the undoped region, depletion region, the well width, the barrier width, and the number of quantum wells are represented as  $d_u$ ,  $d_d$ ,  $L_w$ ,  $L_b$ , and  $N$ , respectively.

Solving Equation (38) with respect to the internal field

$$E_i = \frac{(V_{bi} - E_{piezo}NL_w)}{(d_u + d_d)} \tag{39}$$

and inserting Equation (39) in Equation (37) results in Equation (40), which coincides with Equation (35):

$$E_{total} = \frac{V_{bi} - V_{appl} - E_{piezo}NL_w}{d_u + d_d} + E_{piezo} \tag{40}$$

The internal field  $\vec{E}_i$  is the sum of the fields due to the piezoelectric effect and the spontaneous polarization. The background field written as the total voltage drop divided by the distance, over which that drop occurs, has led to the replacement of the MQW-width  $L = n(L_w + L_b)$  in Equation (35)



by  $(d_u + d_d)$  in Equation (40). Apparently, the width of the intrinsic region  $d_u$  is given by the sum of the unintentionally doped multiple well and barrier widths:

$$d_u = N(L_w + L_b) = L \tag{41}$$

The depletion width  $d_d$  is the sum of the p- and n-type depletion widths and varies with the applied bias. The depletion width  $d_d$ , in a p-i-n structure, can be approximated by [99]:

$$d_d = -d_u + \sqrt{d_u^2 + 2\left(\frac{N_D + N_A}{N_D N_A}\right) \frac{\epsilon_0 \epsilon (V_{bi} - V_{appl} - E_p d_{QW})}{q}} \tag{42}$$

$$d_{QW} = NL_w$$

where  $d_{QW}$  is the sum of the multiple QW widths and  $N_A, N_D$  are the acceptor and donor doping density, respectively.

### 3.5. Electrooptical Response of PIN-Diodes Sensed by Electroluminescence (EL) Spectroscopy

The EL emission spectra of the PIN-diodes based on the GaN reference structure and the  $\text{In}_{0.055}\text{Ga}_{0.945}\text{N}/\text{GaN}$ ,  $\text{In}_{0.15}\text{Al}_{0.85}\text{N}/\text{GaN}$ ,  $\text{In}_{0.18}\text{Al}_{0.82}\text{N}/\text{GaN}$ , and  $\text{In}_{0.21}\text{Al}_{0.79}\text{N}/\text{GaN}$  quantum well heterostructures are presented in Figures 10 and 11; evidently, both the excitonic- and defect-related emission depend on the applied bias-voltage (DC, AC, or a combination of both DC and AC). The excitonic emission in the UV spectral range is facilitated at higher voltages, whereas at voltages slightly above the EL emission-threshold of the PIN-diodes, only the defect-related emission due to the donor–acceptor pair recombination (DAP) in the VIS range is present, as demonstrated in Figure 10a,b.

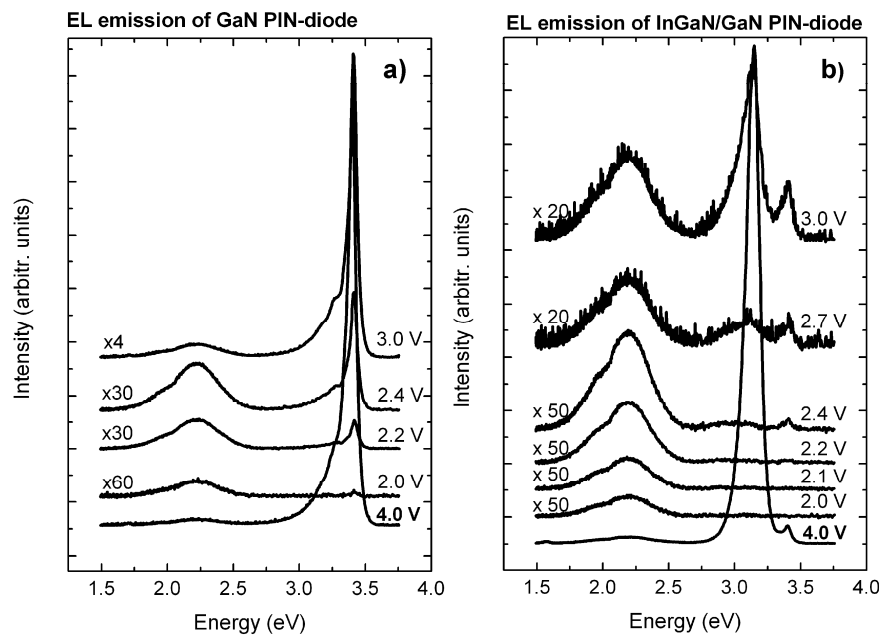


**Figure 10.** EL emission spectra of PIN-diodes based on (a) GaN reference structure and (b)  $\text{In}_{0.055}\text{Ga}_{0.945}\text{N}/\text{GaN}$  DHS in dependence of DC bias-voltage.

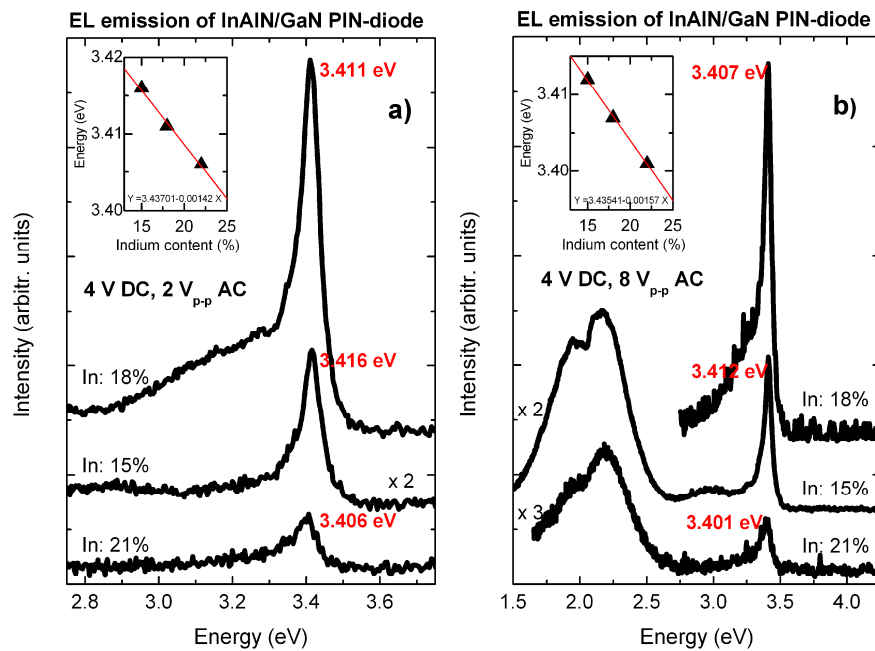


**Figure 11.** EL emission spectra of PIN-diodes based on  $\text{In}_x\text{Al}_{1-x}\text{N}/\text{GaN}$  DHS in dependence of In-fraction  $x = 15, 18,$  and  $21\%$  and AC bias-voltage of (a)  $2 V_{p-p}$  and (b)  $8 V_{p-p}$ .

The EL emission characteristics of PIN-diodes based on the GaN reference structure and the  $\text{In}_{0.055}\text{Ga}_{0.945}\text{N}/\text{GaN}$  DHS exhibit a vast change by variation of the DC voltage in the range 2–4 V under maintenance of the AC voltage at  $2 V_{p-p}$ . An intensity-tuning of the ratio of the excitonic- to defect-related emission in UV–VIS is thus easily achieved in conjunction with the applied forward bias. In fact, group-III nitride based QW heterostructures exhibit much larger optical gains in case the optical matrix element is largely enhanced due to the disappearance of the internal field [111]. The exact emission energies of the EL components in UV–VIS and VIS–NIR were obtained by fitting the EL spectra with Gaussians. In case of the GaN PIN-diode operated at 2.4 V DC and  $2 V_{p-p}$  AC, the UV emission is composed of a high intensity component at the GaN fundamental gap energy  $E_a (=E_0) = 3.414$  eV, with particularly narrow bandwidth (FWHM) of  $\Gamma = 0.054$  eV, and a broader low intensity component at  $E_{DAP} = 3.299$  eV,  $\Gamma = 0.283$  eV. In case of the PIN-diode of the  $\text{In}_{0.055}\text{Ga}_{0.945}\text{N}/\text{GaN}$  DHS, an additional EL component related to the excitonic emission of the InGaN/GaN quantum well heterostructure was observed. Following the trend of the UV emission of GaN, this additional EL band was enhanced as the DC voltage progressively increased.

The EL emission characteristics of PIN-diodes based on the  $\text{In}_{0.15}\text{Al}_{0.85}\text{N}/\text{GaN}$ ,  $\text{In}_{0.18}\text{Al}_{0.82}\text{N}/\text{GaN}$ , and  $\text{In}_{0.21}\text{Al}_{0.79}\text{N}/\text{GaN}$  DHS were shadowed by the emission of the low energy gap GaN over-layers. The excitonic- and defect-related emission of GaN in dependence of the DC voltage, in Figure 11a,b, follows the same trend, as previously discussed. By comparison of the EL emission energy of  $\text{In}_x\text{Al}_{1-x}\text{N}/\text{GaN}$  PIN-diodes with  $x = 0.15, 0.18,$  and  $0.21$ , at a fixed bias-voltage, a red-shift of the GaN barrier emission with the increase of indium content was evidenced, which indicates that the overall emission characteristics of the  $\text{In}_x\text{Al}_{1-x}\text{N}/\text{GaN}$  DHS appear red-shifted by an increase of indium in consistency with published literature [112].

#### 4. Conclusions

Studies of the electro-optical response of PIN-diodes based on  $\text{In}_{0.055}\text{Ga}_{0.945}\text{N}/\text{GaN}$  and  $\text{In}_{0.15}\text{Al}_{0.85}\text{N}/\text{GaN}$ ,  $\text{In}_{0.18}\text{Al}_{0.82}\text{N}/\text{GaN}$ ,  $\text{In}_{0.21}\text{Al}_{0.79}\text{N}/\text{GaN}$  quantum well heterostructures revealed selective excitation of the three valence-split bands of the GaN barrier structure,  $E_a$ ,  $E_b$ , and  $E_c$ , in deep well/shallow barrier InAlN/GaN DHS, which opens new possibilities for the fine adjustment of UV emission components. The strength of the polarization field extracted from the ER spectra of the

$\text{In}_{0.21}\text{Al}_{0.79}\text{N}/\text{GaN}$  DHS  $E_{pol} = 5.4 \pm 1.6$  MV/cm is in excellent agreement with the field value measured by CVM  $E_{pol} = 5.1 \pm 0.8$  MV/cm [45]. The strength and direction of the internal polarization field  $E_{pol} = -2.3 \pm 0.3$  MV/cm determined from Franz–Keldysh oscillations, in the electro-modulated spectra of the  $\text{In}_{0.055}\text{Ga}_{0.945}\text{N}/\text{GaN}$  DHS under flat-barrier conditions, are in agreement, within experimental and calculation errors, with the capacitance-voltage measurement results  $E_{pol} = -1.2 \pm 0.4$  MV/cm, which justifies the application of both optical and electrical characterization techniques for comparative studies of polarization fields in group-III nitrides. In addition, the (total) polarization field strength of  $\text{In}_x\text{Ga}_{1-x}\text{N}$  ( $x = 0.055$ ) obtained by ER and CVM and the strength  $E_{pol} = -0.50 \pm 0.07$  MV/cm obtained by CVM on  $\text{In}_x\text{Ga}_{1-x}\text{N}$  ( $x = 0.08$ ), in a previously published work [46], are in agreement, within statistical fluctuations, with the theoretically predicted values [19,26,38]. As expected, the (absolute) polarization field value extracted from the FKOs of (0001) oriented  $\text{In}_{0.055}\text{Ga}_{0.945}\text{N}/\text{GaN}$ , in this work, is significantly higher than the value  $E_{pol} = -0.575 \pm 0.150$  MV/cm measured by FKOs on a semipolar  $(11\bar{2}2)$  oriented  $\text{In}_{0.12}\text{Ga}_{0.88}\text{N}$  quantum well [99].

**Funding:** The scientific research was funded by the Staff-Mobility Programmes of the European Union.

**Acknowledgments:** This work was elaborated by author D. N. Papadimitriou, staff member of the National Technical University of Athens (NTUA), in the framework of the Staff Mobility Agreement between the NTUA and the Technical University of Berlin (TU-BERLIN) supported by the ERASMUS Programme of the European Union. The group-III nitride based PIN-diodes were provided by TU-BERLIN and its Cooperative Institutions. NTUA staff members Ch. Argiris (Chemical Engineering) and E. Christoforou (Electrical Engineering) are acknowledged for commenting on the PIN-diodes equivalent circuits.

**Conflicts of Interest:** No conflict of interest in relation to the “Calibration of Polarization Fields and Electro-Optical Response of Group-III Nitride Based c-plane Quantum-Well Heterostructures by Application of Electro-Modulation Techniques”.

## References

1. Senoh, M.; Nakamura, S.; Mukai, T. High-power InGaN/GaN double-heterostructure violet light emitting diodes. *Appl. Phys. Lett.* **1993**, *62*, 2390–2392.
2. Kuball, M.; Jeon, E.-S.; Song, Y.-K.; Nurmikko, A.V.; Kozodoy, P.; Abare, A.; Keller, S.; Coldren, L.A.; Mishra, U.K.; DenBaars, S.P.; et al. Gain spectroscopy on InGaN/GaN quantum well diodes. *Appl. Phys. Lett.* **1997**, *70*, 2580–2582. [[CrossRef](#)]
3. Ambacher, O. Growth and applications of Group III-nitrides. *J. Phys. D Appl. Phys.* **1998**, *31*, 2653–2710. [[CrossRef](#)]
4. Ye, P.D.; Yang, B.; Ng, K.K.; Bude, J.; Wilk, G.D.; Halder, S.; Hwang, J.C.M. GaN metal-oxide-semiconductor high-electron-mobility-transistor with atomic layer deposited  $\text{Al}_2\text{O}_3$  as gate dielectric. *Appl. Phys. Lett.* **2005**, *86*, 063501. [[CrossRef](#)]
5. Kaplar, R.J.; Kurtz, S.R.; Koleske, D.D. Novel optical probes of InGaN/GaN light-emitting diodes: 1. Electroreflectance Stark spectroscopy, and 2. Time-resolved emission. *Phys. Status Solidi (C)* **2005**, *2*, 2866–2870. [[CrossRef](#)]
6. Ruterana, P.; Albrecht, M.; Neugebauer, J. (Eds.) *Nitride Semiconductors: Handbook on Materials and Device*; John Wiley & Sons: Hoboken, NJ, USA, 2003.
7. Schubert, E.F. *Light-Emitting Diodes*; Cambridge University Press: Cambridge, UK, 2006.
8. Farrell, R.M.; Neufeld, C.J.; Cruz, S.C.; Lang, J.R.; Iza, M.; Keller, S.; Nakamura, S.; DenBaars, S.P.; Mishra, U.K.; Speck, J.S. High quantum efficiency InGaN/GaN multiple quantum well solar cells with spectral response extending out to 520 nm. *Appl. Phys. Lett.* **2011**, *98*, 201107. [[CrossRef](#)]
9. Morkoç, H. *Handbook of Nitride Semiconductors and Devices, Materials Properties, Physics and Growth*; John Wiley & Son: Hoboken, NJ, USA, 2009.
10. Wu, J. When group-III nitrides go infrared: New properties and perspectives. *J. Appl. Phys.* **2009**, *106*, 11101. [[CrossRef](#)]
11. Sizov, D.; Bhat, R.; Zah, C.E. Gallium Indium Nitride-Based Green Lasers. *J. Lightwave Technol.* **2012**, *5*, 679. [[CrossRef](#)]

12. Willner, A.E.; Byer, R.L.; Chang-Hasnain, C.J.; Forrest, S.R.; Kressel, H.; Kogelnik, H.; Tearney, G.J.; Townes, C.H.; Zervas, M.N. Optics and Photonics: Key Enabling Technologies. *Proc. IEEE* **2012**, *100*, 1604–1643. [[CrossRef](#)]
13. DenBaars, S.P.; Feezell, D.; Kelchner, K.; Pimputkar, S.; Pan, C.-C.; Yen, C.-C.; Tanaka, S.; Zhao, Y.; Pfaff, N.; Farrell, R.; et al. Development of gallium-nitride-based light-emitting diodes (LEDs) and laser diodes for energy-efficient lighting and displays. *Acta Mater.* **2013**, *61*, 945–951. [[CrossRef](#)]
14. Hatakeyama, Y.; Nomoto, K.; Terano, A.; Kaneda, N.; Tsuchiya, T.; Mishima, T.; Nakamura, T. High-Breakdown-Voltage and Low-Specific-on-Resistance GaN p–n Junction Diodes on Free-Standing GaN Substrates Fabricated Through Low-Damage Field-Plate Process. *Jpn. J. Appl. Phys.* **2013**, *52*, 28007. [[CrossRef](#)]
15. Krishnamoorthy, S.; Akyol, F.; Park, P.S.; Rajan, S. Low resistance GaN/InGaN/GaN tunnel junctions. *Appl. Phys. Lett.* **2013**, *102*, 113503. [[CrossRef](#)]
16. Kneissl, M.; Rass, J. (Eds.) *III-Nitride Ultraviolet Emitters: Technology and Applications*; Springer: Berlin/Heidelberg, Germany, 2016.
17. Huang, J.J.; Kuo, H.C.; Shen, S.C. *Nitride Semiconductor Light-Emitting Diodes (LEDs): Materials, Technologies and Applications*; Woodhead Publishing: Sawston, UK, 2016.
18. Ferreyra, R.A.; Zhu, C.; Teke, A.; Morkoç, H. Group III Nitrides. In *Springer Handbook of Electronic and Photonic Materials*; Kasap, S., Capper, P., Eds.; Springer: Berlin/Heidelberg, Germany, 2017.
19. Bernardini, F.; Fiorentini, V.; Vanderbilt, D. Spontaneous polarization and piezoelectric constants of III-V nitrides. *Phys. Rev. B* **1997**, *56*, R10024. [[CrossRef](#)]
20. Takeuchi, Y.; Sota, S.; Katsuragawa, M.; Komori, M.; Takeuchi, H.; Amano, H.; Akasaki, I. Theoretical Study of Orientation Dependence of Piezoelectric Effects in Wurtzite Strained GaInN/GaN Heterostructures and Quantum Wells. *Jpn. J. Appl. Phys.* **1997**, *36*, 382. [[CrossRef](#)]
21. Yu, E.T.; Dang, X.Z.; Asbeck, P.M.; Lau, S.S.; Sullivan, G.J. Spontaneous and piezoelectric polarization effects in III–V nitride heterostructures. *J. Vac. Sci. Technol. B* **1999**, *17*, 1742. [[CrossRef](#)]
22. Bernardini, F.; Fiorentini, V.; Vanderbilt, D. Accurate calculation of polarization-related quantities in semiconductors. *Phys. Rev. B* **2001**, *63*, 193201. [[CrossRef](#)]
23. Zoroddu, A.; Bernardini, F.; Fiorentini, V.; Ruggerone, P. First-principles prediction of structure, energetics, formation enthalpy, elastic constants, polarization, and piezoelectric constants of AlN, GaN, and InN: Comparison of local and gradient-corrected density-functional theory. *Phys. Rev. B* **2001**, *64*, 045208. [[CrossRef](#)]
24. Bernardini, F.; Fiorentini, V. Nonlinear macroscopic polarization in III-V nitride alloys. *Phys. Rev. B* **2001**, *64*, 129903. [[CrossRef](#)]
25. Bernardini, F.; Fiorentini, V.; Ambacher, O. Evidence for nonlinear macroscopic polarization in III–V nitride alloy heterostructures. *Appl. Phys. Lett.* **2002**, *80*, 1204–1206.
26. Ambacher, O.; Miskys, C.; Eickhoff, M.; Bernardini, F.; Tilak, V.; Eastman, L.F.; Majewski, J.; Link, A.; Hermann, M.; Stutzmann, M.; et al. Pyroelectric properties of Al(In)GaN/GaN hetero- and quantum well structures. *J. Phys. Condens. Matter* **2002**, *14*, 3399–3434. [[CrossRef](#)]
27. Li, J.M.; Lü, Y.W.; Li, D.B.; Han, X.X.; Zhu, Q.S.; Liu, X.L.; Wang, Z.G. Effect of spontaneous and piezoelectric polarization on intersubband transition in  $\text{Al}_x\text{Ga}_{1-x}\text{N}$ -GaN quantum well. *J. Vac. Sci. Technol. B Microelectron. Nanometer Struct.* **2004**, *22*, 2568. [[CrossRef](#)]
28. Brown, I.H.; Pope, I.A.; Smowton, P.M.; Blood, P.; Thomson, J.D.; Chow, W.W.; Bour, D.P.; Kneissl, M. Determination of the piezoelectric field in InGaN quantum wells. *Appl. Phys. Lett.* **2005**, *86*, 131108. [[CrossRef](#)]
29. Feneberg, M.; Thonke, K. Polarization fields of III-nitrides grown in different crystal orientations. *J. Phys. Condens. Matter* **2007**, *19*, 403201. [[CrossRef](#)] [[PubMed](#)]
30. Schwarz, U.T.; Kneissl, M. Nitride emitters go nonpolar. *Phys. Status Solidi (RRL)-Rapid Res. Lett.* **2007**, *1*, A44–A46. [[CrossRef](#)]
31. Xu, D.; He, H.; Pandey, R.; Karna, S.P. Stacking and electric field effects in atomically thin layers of GaN. *J. Phys. Condens. Matter* **2013**, *25*, 345302. [[CrossRef](#)] [[PubMed](#)]
32. Ibbetson, J.P.; Fini, P.T.; Ness, K.D.; DenBaars, S.P.; Speck, J.S.; Mishra, U.K. Polarization effects, surface states, and the source of electrons in AlGaIn/GaN heterostructure field effect transistors. *Appl. Phys. Lett.* **2000**, *77*, 250–252. [[CrossRef](#)]

33. Hanada, T. Basic Properties of ZnO, GaN, and Related Materials. In *Oxide and Nitride Semiconductors*; Yao, T., Hong, S.K., Eds.; Springer: Berlin/Heidelberg, Germany, 2009.
34. Dreyer, C.E.; Janotti, A.; Van De Walle, C.G.; Vanderbilt, D. Correct Implementation of Polarization Constants in Wurtzite Materials and Impact on III-Nitrides. *Phys. Rev. X* **2016**, *6*, 021038. [[CrossRef](#)]
35. Kisielowski, C.; Krüger, J.; Ruvimov, S.; Suski, T.; Ager, J.W., III; Jones, E.; Liliental-Weber, Z.; Rubin, M.; Weber, E.R.; Bremser, M.D.; et al. Strain-related phenomena in GaN thin films. *Phys. Rev. B* **1996**, *54*, 17745. [[CrossRef](#)]
36. Lorenz, K.; Franco, N.; Alves, E.; Watson, I.M.; Martin, R.W.; O'Donnell, K.P. Anomalous Ion Channeling in AlInN/GaN Bilayers: Determination of the Strain State. *Phys. Rev. Lett.* **2006**, *97*, 085501. [[CrossRef](#)]
37. Lorenz, K.; Franco, N.; Alves, E.; Pereira, S.; Watson, I.; Martin, R.; O'Donnell, K. Relaxation of compressively strained AlInN on GaN. *J. Cryst. Growth* **2008**, *310*, 4058–4064. [[CrossRef](#)]
38. Wright, A.F. Elastic properties of zinc-blende and wurtzite AlN, GaN, and InN. *J. Appl. Phys.* **1997**, *82*, 2833–2839. [[CrossRef](#)]
39. Böttger, H.; Bryksin, V.V. Hopping conductivity in ordered and disordered solids (I). *Phys. Status Solidi (b)* **1976**, *78*, 9–56. [[CrossRef](#)]
40. Takeuchi, T.; Sota, S.; Katsuragawa, M.; Komori, M.; Takeuchi, H.; Amano, H.; Akasaki, I. Quantum-Confined Stark Effect due to Piezoelectric Fields in GaInN Strained Quantum Wells. *Jpn. J. Appl. Phys.* **1997**, *36*, L382. [[CrossRef](#)]
41. Wetzel, C.; Takeuchi, T.; Amano, H.; Akasaki, I. Piezoelectric Stark-like Ladder in GaN/GaInN/GaN Heterostructures. *Jpn. J. Appl. Phys.* **1999**, *38*, L163. [[CrossRef](#)]
42. Dong, L.; Yadav, S.; Ramprasad, R.; Alpay, S.P. Band gap tuning in GaN through equibiaxial in-plane strains. *Appl. Phys. Lett.* **2010**, *96*, 202106. [[CrossRef](#)]
43. Yan, Q.; Rinke, P.; Janotti, A.; Scheffler, M.; Van De Walle, C.G. Effects of strain on the band structure of group-III nitrides. *Phys. Rev. B* **2014**, *90*, 125118. [[CrossRef](#)]
44. Roumeliotis, G.G. MSc-thesis (English) III-Nitride Emitters and Converters: Built-in Polarization-Induced Electric Fields, Built-in Potential, and Effective Doping Concentration. Master's Thesis, National Technical University of Athens, Interdisciplinary Interdepartmental Postgraduate Program Materials Science and Technology, Athens, Greece, 2017.
45. Susilo, N.; Roumeliotis, G.; Narodovitch, M.; Witzigmann, B.; Rychetsky, M.; Neugebauer, S.; Gutmann, M.; Enslin, J.; Dadgar, A.; Niermann, T.; et al. Accurate determination of polarization fields in (0001) c-plane InAlN/GaN heterostructures with capacitance-voltage-measurements. *J. Phys. D Appl. Phys.* **2018**, *51*, 485103. [[CrossRef](#)]
46. Rychetsky, M.; Koslow, I.; Avinc, B.; Rass, J.; Wernicke, T.; Bellmann, K.; Sulmoni, L.; Hoffmann, V.; Weyers, M.; Wild, J.; et al. Determination of polarization fields in group III-nitride heterostructures by capacitance-voltage-measurements. *J. Appl. Phys.* **2016**, *119*, 095713. [[CrossRef](#)]
47. Gessmann, T.; Graff, J.W.; Waldron, E.L.; Schubert, E.F.; Li, Y.-L. Ohmic contact technology in III nitrides using polarization effects of cap layers. *J. Appl. Phys.* **2002**, *92*, 3740–3744. [[CrossRef](#)]
48. Schubert, E.F.; Kopf, R.F.; Kuo, J.M.; Luftman, H.S.; Garbinski, P.A. Spatial resolution of the capacitance-voltage profiling technique on semiconductors with quantum confinement. *Appl. Phys. Lett.* **1990**, *57*, 497–499. [[CrossRef](#)]
49. Schubert, E.F.; Kuo, J.M.; Kopf, R.F. Theory and experiment of capacitance-voltage profiling on semiconductors with quantum-confinement. *J. Electron. Mater.* **1990**, *19*, 521–531. [[CrossRef](#)]
50. Rimmer, J.S.; Hamilton, B.; Peaker, A.R. *Capacitance-Voltage Profiling of Multilayer Semiconductor Structures in Low-Dimensional Structures in Semiconductors*; Springer: Berlin/Heidelberg, Germany, 1991; pp. 139–146.
51. Iniewski, K. Optimization of the capacitance–voltage profiling method based on inverse modeling. *J. Vac. Sci. Technol. B Microelectron. Nanometer Struct.* **1992**, *10*, 480. [[CrossRef](#)]
52. Sundaram, M.; Gossard, A.C. Capacitance-voltage profiling through graded heterojunctions: Theory and experiment. *J. Appl. Phys.* **1993**, *73*, 251–260. [[CrossRef](#)]
53. Tschirner, B.M.; Morier-Genoud, F.; Martin, D.; Reinhart, F.K. Capacitance-voltage profiling of quantum well structures. *J. Appl. Phys.* **1996**, *79*, 7005–7013. [[CrossRef](#)]
54. Bobylev, B.; Kovalevskaja, T.; Marchishin, I.; Ovsyuk, V. Capacitance-voltage profiling of multiquantum well structures. *Solid State Electron.* **1997**, *41*, 481–486. [[CrossRef](#)]

55. Reynolds, N.D.; Panda, C.D.; Essick, J.M. Capacitance-voltage profiling: Research-grade approach versus low-cost alternatives. *Am. J. Phys.* **2014**, *82*, 196–205. [[CrossRef](#)]
56. Aghaei, S.; Hehta, M.; Andrei, P.; Hagmann, M.J. Challenges and opportunities in atomistic dopant profiling using capacitance-voltage measurements. In Proceedings of the 25th Annual SEMI Advanced Semiconductor Manufacturing Conference (ASMC 2014), Institute of Electrical and Electronics Engineers, Saratoga Springs, NY, USA, 19–21 May 2014; pp. 130–135.
57. Biswas, D.; Panda, S. An effective approach for the minimization of errors in capacitance-voltage carrier profiling of quantum structures. *J. Appl. Phys.* **2014**, *115*, 134308. [[CrossRef](#)]
58. Watanabe, M.O.; Ohba, Y. Interface properties for GaAs/InGaAlP heterojunctions by the capacitance-voltage profiling technique. *Appl. Phys. Lett.* **1987**, *50*, 906–908. [[CrossRef](#)]
59. Knübel, A.; Polyakov, V.M.; Kirste, L.; Aidam, R. Nonuniformity of electron density in In-rich InGaN films deduced from electrolyte capacitance-voltage profiling. *Appl. Phys. Lett.* **2010**, *96*, 82106. [[CrossRef](#)]
60. Wang, X.-H.; Zhao, M.; Liu, X.-Y.; Pu, Y.; Zheng, Y.-K.; Wei, K. The physical process analysis of the capacitance—Voltage characteristics of AlGaN/AlN/GaN high electron mobility transistors. *Chin. Phys. B* **2010**, *19*, 97302.
61. Suzuki, M.; Uenoyama, T.; Yanase, A. First-principles calculations of effective-mass parameters of AlN and GaN. *Phys. Rev. B* **1995**, *52*, 8132–8139. [[CrossRef](#)] [[PubMed](#)]
62. Suzuki, M.; Uenoyama, T. First principles calculation of effective mass parameters of GaN. *Solid State Electron.* **1997**, *41*, 271–274. [[CrossRef](#)]
63. Yeo, Y.C.; Chong, T.C.; Li, M.F. Electronic band structures and effective-mass parameters of wurtzite GaN and InN. *J. Appl. Phys.* **1998**, *83*, 1429–1436. [[CrossRef](#)]
64. Vurgaftman, I.; Meyer, J.R. Band parameters for nitrogen-containing semiconductors. *J. Appl. Phys.* **2003**, *94*, 3675–3696. [[CrossRef](#)]
65. Sze, S.M.; Ng, K.K. *Physics of Semiconductor Devices*; John Wiley & Sons: Hoboken, NJ, USA, 2006.
66. Peter, Y.U.; Cardona, M. *Fundamentals of Semiconductors: Physics and Materials Properties*; Springer: Berlin/Heidelberg, Germany, 2010.
67. Shan, W.; Schmidt, T.J.; Song, J.J.; Goldenberg, B.; Yang, X.H.; Hwang, S.J. Temperature dependence of interband transitions in GaN grown by metalorganic chemical vapor deposition. *Appl. Phys. Lett.* **1995**, *66*, 985–987. [[CrossRef](#)]
68. Moses, P.G.; Miao, M.; Yan, Q.; Van De Walle, C. Hybrid functional investigations of band gaps and band alignments for AlN, GaN, InN, and InGaN. *J. Chem. Phys.* **2011**, *134*, 84703. [[CrossRef](#)]
69. Yamaguchi, S.; Sakai, H.; Kaneko, Y.; Nakagawa, S.; Yamaoka, Y.; Takeuchi, T.; Wetzel, C.; Amano, H.; Akasaki, I.; Yamada, N. Determination of piezoelectric fields in strained GaInN quantum wells using the quantum-confined Stark effect. *Appl. Phys. Lett.* **1998**, *73*, 1691–1693.
70. Jho, Y.D.; Yahng, J.S.; Oh, E.; Kim, D.S. Field-dependent carrier decay dynamics in strained  $\text{In}_x\text{Ga}_{1-x}\text{N}/\text{GaN}$  quantum wells. *Phys. Rev. B* **2002**, *66*, 035334. [[CrossRef](#)]
71. Goossen, K.W.; Caridi, E.A.; Chang, T.Y.; Stark, J.B.; Miller, D.A.B.; Morgan, R.A. Observation of room-temperature blue shift and bistability in a strained InGaAs-GaAs (111) self-electro-optic effect device. *Appl. Phys. Lett.* **1990**, *56*, 715–717. [[CrossRef](#)]
72. Pabla, A.S.; Sanchez-Rojas, J.L.; Woodhead, J.; Grey, R.; David, J.P.R.; Rees, G.J.; Hill, G.; Pate, M.A.; Robson, P.N.; Hogg, R.A.; et al. Tailoring of internal fields in InGaAs/GaAs multiwell structures grown on (111)B GaAs. *Appl. Phys. Lett.* **1993**, *63*, 752–754. [[CrossRef](#)]
73. David, J.P.R.; Sale, T.E.; Pabla, A.S.; Rodríguez-Gironés, P.J.; Woodhead, J.; Grey, R.; Rees, G.J.; Robson, P.N.; Skolnick, M.; Hogg, R.A. Excitation power and barrier width dependence of photoluminescence in piezoelectric multiquantum well p-i-n structures. *Appl. Phys. Lett.* **1996**, *68*, 820–822. [[CrossRef](#)]
74. Li, C.F.; Huang, Y.S.; Malikova, L.; Pollak, F.H. Temperature dependence of the energies and broadening parameters of the interband excitonic transitions in wurtzite GaN. *Phys. Rev. B* **1997**, *55*, 9251–9254. [[CrossRef](#)]
75. Shokhovets, S.; Goldhahn, R.; Gobsch, G. Study of the linear electro-optic effect in  $\alpha$ -GaN by electroreflectance. *Mater. Sci. Eng. B* **2002**, *93*, 215–218. [[CrossRef](#)]
76. Wickenden, A.E.; Koleske, D.D.; Al-Kuhaili, M.; Glosser, R.; Henry, R.L. Electroreflectance of hexagonal gallium nitride at the fundamental and E 1 spectral regions. *Appl. Phys. Lett.* **2003**, *82*, 1203–1205.
77. Kaplar, R.J. Electroreflectance studies of Stark shifts and polarization-induced electric fields in InGaN/GaN single quantum wells. *J. Appl. Phys.* **2004**, *95*, 4905. [[CrossRef](#)]

78. Yoon, J.W.; Kim, S.S.; Cheong, H.S.; Seo, H.C.; Kwon, S.Y.; Kim, H.J.; Shin, Y.R.; Yoon, E.J.; Park, Y.S. Electroreflectance and Photoluminescence Study on InGaN Alloys. *J. Korean Phys. Soc.* **2006**, *49*, 2143–2146.
79. Drabinska, A.; Korona, K.P.; Pakula, K.; Baranowski, J.M. Electroreflectance and photorefectance spectra of tricolor III-nitride detector structures. *Phys. Status Solidi (a)* **2007**, *204*, 459–465. [[CrossRef](#)]
80. Avakyants, L.P.; Badgutdinov, M.L.; Bokov, P.Y.; Chervyakov, A.V.; Shirokov, S.S.; Yunovich, A.E.; Bogdanov, A.A.; Vasil'Eva, E.D.; Nikolaev, D.A.; Feopentov, A.V. Electroreflectance spectra of InGaN/AlGaIn/GaN quantum-well heterostructures. *Semiconductors* **2007**, *41*, 1060–1066. [[CrossRef](#)]
81. Kudrawiec, R.; Siekacz, M.; Kryśko, M.; Cywiński, G.; Misiewicz, J.; Skierbiszewski, C. Contactless electroreflectance of InGaIn layers with indium content  $\leq 36\%$ : The surface band bending, band gap bowing, and Stokes shift issues. *J. Appl. Phys.* **2009**, *106*, 113517. [[CrossRef](#)]
82. Avakyants, L.; Bokov, P.; Chervyakov, A.; Chuas, A.; Yunovich, A.; Vasileva, E.; Yavich, B. Electroreflectance diagnostics of InGaIn/AlGaIn/GaN based LEDs structures. *Phys. Status solidi (c)* **2009**, *6*, 2852–2854. [[CrossRef](#)]
83. Tawfik, W.Z.; Ryu, H.-Y.; Lee, J.K. Electroreflectance spectroscopy of compressively strained InGaIn/GaN multi-quantum well structures. *Curr. Appl. Phys.* **2014**, *14*, 1504–1508. [[CrossRef](#)]
84. Aspnes, D.; Bottka, N. Chapter 6 Electric-Field Effects on the Dielectric Function of Semiconductors and Insulators. *Semicond. Semimet.* **1972**, *9*, 457–543.
85. Aspnes, D. Third-derivative modulation spectroscopy with low-field electroreflectance. *Surf. Sci.* **1973**, *37*, 418–442. [[CrossRef](#)]
86. Aspnes, D.E. Modulation Spectroscopy/Electric Field Effects on the Dielectric Function of Semiconductors. In *Handbook on Semiconductors*; Moss, T.S., Balkanski, M., Eds.; North Holland Publishing: Amsterdam, The Netherlands, 1980.
87. Klipstein, P.C.; Tapster, P.R.; Apsley, N.; Skolnick, M.; Kerr, T.M.; Woodbridge, K.; Anderson, D. Electroreflectance spectroscopy from quantum well structures in an electric field. *J. Phys. C Solid State Phys.* **1986**, *19*, 857–871. [[CrossRef](#)]
88. Klipstein, P.C.; Apsley, N. A theory for the electroreflectance spectra of quantum well structures. *J. Phys. C Solid State Phys.* **1986**, *19*, 6461–6478. [[CrossRef](#)]
89. Thorn, A.P.; Shields, A.J.; Klipstein, P.C.; Apsley, N.; Kerr, T.M. The electro-reflectance lineshape for a quantum well: The dependence on angle of incidence and temperature. *J. Phys. C Solid State Phys.* **1987**, *20*, 4229–4239. [[CrossRef](#)]
90. Pollak, F.H.; Shen, H. Modulation spectroscopy of semiconductors: Bulk/thin film, microstructures, surfaces/interfaces and devices. *Mater. Sci. Eng. R: Rep.* **1993**, *10*, 275. [[CrossRef](#)]
91. Pollak, F.H. Modulation Spectroscopy of Semiconductor and Semiconductor Microstructures. In *Optical Properties of Semiconductors*; Balkanski, M., Ed.; North Holland Publishing: Amsterdam, The Netherlands, 1994; Volume 2.
92. Pollak, F.H. Study of semiconductor surfaces and interfaces using electromodulation. *Surf. Interface Anal.* **2001**, *31*, 938–953. [[CrossRef](#)]
93. Misiewicz, J.; Kudrawiec, R. Contactless electroreflectance spectroscopy of optical transitions in low dimensional semiconductor structures. *Opto Electron. Rev.* **2012**, *20*, 101–119. [[CrossRef](#)]
94. Aspnes, D.E. Band nonparabolicities, broadening, and internal field distributions: The spectroscopy of Franz-Keldysh oscillations. *Phys. Rev. B* **1974**, *10*, 4228–4238. [[CrossRef](#)]
95. Shen, H.; Pollak, F.H. Generalized Franz-Keldysh theory of electromodulation. *Phys. Rev. B* **1990**, *42*, 7097–7102. [[CrossRef](#)] [[PubMed](#)]
96. Batchelor, R.A.; Hamnett, A. A Franz-Keldysh model for photorefectance from GaAs/GaAlAs heterojunction structures. *J. Appl. Phys.* **1992**, *71*, 2414–2422. [[CrossRef](#)]
97. Shen, H.; Dutta, M.; Chang, W.; Moerkirk, R.; Kim, D.M.; Chung, K.W.; Ruden, P.P.; Nathan, M.I.; Stroscio, M.A. Direct measurement of piezoelectric field in a [111]B grown InGaAs/GaAs heterostructure by Franz–Keldysh oscillations. *Appl. Phys. Lett.* **1992**, *60*, 2400–2402. [[CrossRef](#)]
98. Wetzels, C.; Takeuchi, T.; Amano, H.; Akasaki, I. Piezoelectric Franz–Keldysh effect in strained GaInN/GaN heterostructures. *J. Appl. Phys.* **1999**, *85*, 3786–3791. [[CrossRef](#)]
99. Shen, H.; Wraback, M.; Zhong, H.; Tyagi, A.; DenBaars, S.P.; Nakamura, S.; Speck, J.S. Determination of polarization field in a semipolar (11 $\bar{2}2$ ) InGaIn/GaN single quantum well using Franz–Keldysh oscillations in electroreflectance. *Appl. Phys. Lett.* **2009**, *94*, 241906. [[CrossRef](#)]

100. Adachi, S. *III-V Ternary and Quaternary Compounds in Springer Handbook of Electronic and Photonic Materials*; Kasap, S., Capper, P., Eds.; Springer: Berlin/Heidelberg, Germany, 2017.
101. Börnstein, L. *Group III Condensed Matter Semiconductors Group IV Elements, IV-IV and III-V Compounds. Part b-Electronic, Transport, Optical and Other Properties*; Madelung, O., Rössler, U., Schulz, M., Eds.; Springer: Berlin/Heidelberg, Germany, 2002; Volume 41.
102. Wilkins, N. Infra-red interference measurements on oxide films on zirconium. *Corros. Sci.* **1964**, *4*, 17–24. [[CrossRef](#)]
103. Kallergi, N.; Roughani, B.; Aubel, J.; Sundaram, S. Correlation of interference effects in photoreflectance spectra with GaAs homolayer thickness. *J. Appl. Phys.* **1990**, *68*, 4656–4661. [[CrossRef](#)]
104. Clark, T.J.; Banash, M.A.; Cruse, R.W.; Fech, J.; Mininni, R.M.; Rohman, S.J. The use of infrared interference spectra to measure ceramic coating thickness in a CVD reactor. *Thin Solid Films* **1995**, *254*, 7–9. [[CrossRef](#)]
105. Losurdo, M.; Bergmair, M.; Bruno, G.; Cattelan, D.; Cobet, C.; de Martino, A.; Fleischer, K.; Dohcevic-Mitrovic, Z.; Esser, N.; Galliet, M.; et al. Spectroscopic ellipsometry and polarimetry for materials and systems analysis at the nanometer scale: state-of-the-art, potential, and perspectives. *J. Nanopart. Res.* **2009**, *11*, 1521–1554. [[CrossRef](#)]
106. Leung, M.M.Y.; Djurišić, A.B.; Li, E.H. Refractive index of InGa<sub>x</sub>N/GaN quantum well. *J. Appl. Phys.* **1998**, *84*, 6312–6317. [[CrossRef](#)]
107. Yang, T.; Goto, S.; Kawata, M.; Uchida, K.; Niwa, A.; Gotoh, J. Optical Properties of GaN Thin Films on Sapphire Substrates Characterized by Variable-Angle Spectroscopic Ellipsometry. *Jpn. J. Appl. Phys.* **1998**, *37*, L1105–L1108. [[CrossRef](#)]
108. Goldhahn, R.; Scheiner, J.; Shokhovets, S.; Frey, T.; Köhler, U.; As, D.J.; Lischka, K. Refractive index and gap energy of cubic In<sub>x</sub>Ga<sub>1-x</sub>N. *Appl. Phys. Lett.* **2000**, *76*, 291–293. [[CrossRef](#)]
109. Laws, G.M.; Larkins, E.C.; Harrison, I.; Molloy, C.; Somerford, D. Improved refractive index formulas for the Al<sub>x</sub>Ga<sub>1-x</sub>N and In<sub>y</sub>Ga<sub>1-y</sub>N alloys. *J. Appl. Phys.* **2001**, *89*, 1108–1115. [[CrossRef](#)]
110. Moustakas, T.D.; Paiella, R. Optoelectronic device physics and technology of nitride semiconductors from the UV to the terahertz. *Rep. Prog. Phys.* **2017**, *80*, 106501. [[CrossRef](#)]
111. Park, S.-H.; Ahn, D.; Kim, J.-W. Optical gain in quantum well structures with zero internal field. *Appl. Phys. Lett.* **2008**, *92*, 171115. [[CrossRef](#)]
112. Wernicke, T.; Schade, L.; Netzel, C.; Rass, J.; Hoffmann, V.; Ploch, S.; Knauer, A.; Weyers, M.; Schwarz, U.; Kneissl, M. Indium incorporation and emission wavelength of polar, nonpolar and semipolar InGa<sub>x</sub>N quantum wells. *Semicond. Sci. Technol.* **2012**, *27*, 024014. [[CrossRef](#)]



© 2019 by the author. Licensee MDPI, Basel, Switzerland. This article is an open access article distributed under the terms and conditions of the Creative Commons Attribution (CC BY) license (<http://creativecommons.org/licenses/by/4.0/>).